



UNIVERSITY OF LEEDS

This is a repository copy of *Fraction-specific controls on the trace element distribution in iron formations: Implications for trace metal stable isotope proxies*.

White Rose Research Online URL for this paper:  
<http://eprints.whiterose.ac.uk/122801/>

Version: Accepted Version

---

**Article:**

Oonk, PBH, Tsikos, H, Mason, PRD et al. (5 more authors) (2017) Fraction-specific controls on the trace element distribution in iron formations: Implications for trace metal stable isotope proxies. *Chemical Geology*, 474. pp. 17-32. ISSN 0009-2541

<https://doi.org/10.1016/j.chemgeo.2017.10.018>

---

© 2017 Elsevier B.V. This manuscript version is made available under the CC-BY-NC-ND 4.0 license <http://creativecommons.org/licenses/by-nc-nd/4.0/>

**Reuse**

Items deposited in White Rose Research Online are protected by copyright, with all rights reserved unless indicated otherwise. They may be downloaded and/or printed for private study, or other acts as permitted by national copyright laws. The publisher or other rights holders may allow further reproduction and re-use of the full text version. This is indicated by the licence information on the White Rose Research Online record for the item.

**Takedown**

If you consider content in White Rose Research Online to be in breach of UK law, please notify us by emailing [eprints@whiterose.ac.uk](mailto:eprints@whiterose.ac.uk) including the URL of the record and the reason for the withdrawal request.

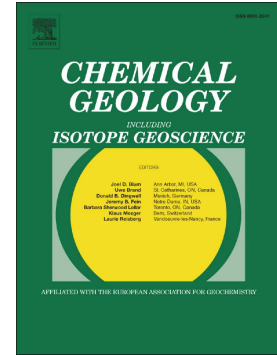


[eprints@whiterose.ac.uk](mailto:eprints@whiterose.ac.uk)  
<https://eprints.whiterose.ac.uk/>

# Accepted Manuscript

Fraction-specific controls on the trace element distribution in iron formations: Implications for trace metal stable isotope proxies

P.B.H. Oonk, H. Tsikos, P.R.D. Mason, S. Henkel, M. Staubwasser, L. Fryer, S.W. Poulton, H.M. Williams



PII: S0009-2541(17)30582-X  
DOI: doi:[10.1016/j.chemgeo.2017.10.018](https://doi.org/10.1016/j.chemgeo.2017.10.018)  
Reference: CHEMGE 18507

To appear in: *Chemical Geology*

Received date: 15 June 2017  
Revised date: 9 October 2017  
Accepted date: 14 October 2017

Please cite this article as: P.B.H. Oonk, H. Tsikos, P.R.D. Mason, S. Henkel, M. Staubwasser, L. Fryer, S.W. Poulton, H.M. Williams, Fraction-specific controls on the trace element distribution in iron formations: Implications for trace metal stable isotope proxies. The address for the corresponding author was captured as affiliation for all authors. Please check if appropriate. *Chemge*(2017), doi:[10.1016/j.chemgeo.2017.10.018](https://doi.org/10.1016/j.chemgeo.2017.10.018)

This is a PDF file of an unedited manuscript that has been accepted for publication. As a service to our customers we are providing this early version of the manuscript. The manuscript will undergo copyediting, typesetting, and review of the resulting proof before it is published in its final form. Please note that during the production process errors may be discovered which could affect the content, and all legal disclaimers that apply to the journal pertain.

## FRACTION-SPECIFIC CONTROLS ON THE TRACE ELEMENT DISTRIBUTION IN IRON FORMATIONS: IMPLICATIONS FOR TRACE METAL STABLE ISOTOPE PROXIES

P.B.H. Oonk<sup>a,b,\*</sup>, H. Tsikos<sup>a</sup>, P.R.D. Mason<sup>b</sup>, S. Henkel<sup>c,d</sup>, M. Staubwasser<sup>c</sup>, L. Fryer<sup>a</sup>, S.W. Poulton<sup>e</sup> and H.M. Williams<sup>f,1</sup>

<sup>a</sup> Geology Department, Rhodes University, Artillery Road, Grahamstown, 6140, South Africa

<sup>b</sup> Department of Earth Sciences, Universiteit Utrecht, Budapestlaan 4, 3584CD Utrecht, The Netherlands

<sup>c</sup> Institute of Geology and Mineralogy, University of Cologne, Zùlpicher Str. 49a, 50674 Cologne, Germany

<sup>d</sup> Alfred Wegener Institute, Helmholtz Centre for Polar and Marine Research, Am Handelshafen 12, 27570 Bremerhaven, Germany

<sup>e</sup> School of Earth and Environment, University of Leeds, Leeds LS2 9JT, United Kingdom

<sup>f</sup> Department of Earth Sciences, Durham University, DH1 3LE, United Kingdom

### ABSTRACT

Iron formations (IFs) are important geochemical repositories that provide constraints on atmospheric and ocean chemistry, prior to and during the onset of the Great Oxidation Event. Trace metal abundances and their Mo-Cr-U isotopic ratios have been widely used for investigating ocean redox processes through the Archean and Paleoproterozoic. Mineralogically, IFs consist of three main Fe-bearing fractions: (1) Fe-Ca-Mg-Mn carbonates, (2) magnetite and/or hematite and (3) Fe-silicates. These fractions are typically fine-grained on a sub- $\mu\text{m}$  scale and their co-occurrence in varying amounts means that bulk-rock or microanalytical geochemical and stable isotope data can be influenced by cryptic changes in mineralogy. Fraction specific geochemical analysis has the potential to resolve mineralogical controls and reveal diagenetic versus primary precipitative controls on IF mineralogy. Here we adapt an existing sequential extraction scheme for Fe-phases (Poulton and Canfield, 2005) to the high Fe-content in IF and the specific three-fraction mineralogy. We optimized the scheme for magnetite-dominated Archean IFs using samples from the hematite-poor Asbestos Hills Subgroup IF, Transvaal Supergroup, South Africa. Previously commonly-used hydroxylamine-HCl

---

\* Corresponding author: Department of Earth Sciences, Universiteit Utrecht, Budapestlaan 4, 3584CD Utrecht, The Netherlands E-mail: [pbhoonk@gmail.com](mailto:pbhoonk@gmail.com).

<sup>1</sup> Current address: Department of Earth Sciences, University of Cambridge, Downing Street, Cambridge, CB2 3EQ, United Kingdom

and dithionite leaches were omitted since ferric oxides are quantitatively insignificant in these IF samples. The acetate leach was tested at variable temperatures, reaction times and under different atmospheres in order to ensure that all micro-crystalline Fe-carbonates were effectively dissolved, resulting in an optimum extraction for 48 hr at 50 °C under anoxic conditions. The dissolution of magnetite by  $\text{NH}_4$ -oxalate was also tested, resulting in an optimum extraction for 24 hr under an ambient atmosphere. Finally, a  $\text{HF-HClO}_4\text{-HNO}_3$  leach was used to dissolve the residual silicate fraction which has to date not been considered in detail in IF. Accuracy of the extraction technique was generally excellent, as verified using 1) elemental recoveries, 2) comparison of major and trace element distributions against mineralogy and 3) comparison to results from microanalytical techniques.

This study focuses on the distribution of three frequently used geochemical proxies in IF; U, Mo and Cr. Molybdenum abundances in the Kuruman and Griquatown IF are low and show an apparent correlation with mineralogical variability, as determined by the sequential extraction. This suggests that changes in bulk-rock mineralogy, rather than redox chemistry might significantly affect Mo stable isotopes. For Cr, a minor bulk-rock stratigraphic increase can be related to the oxide and silicate fraction. However, a positive relationship with Zr indicates that this was also controlled by detrital or volcanic ash input. Uranium is predominantly bound to the silicate fraction and shows clear correlations with Zr and Sc implying detrital reworking under anoxic conditions. The discrepant behaviour of these three proxies indicate that mineralogy should be taken into account when interpreting heterogeneous bulk-rock samples and that fraction specific techniques will provide new insights into the evolution of atmosphere and ocean chemistry.

**KEYWORDS:**

- Iron formation
- Paleoproterozoic
- Sequential extraction
- Trace element speciation
- Transvaal Supergroup

**HIGHLIGHTS:**

- Optimization of a sequential extraction scheme for iron formations
- Procedure gives excellent recovery for the major and trace elements
- Low molybdenum contents in IF show an apparent correlation with mineralogical variability

- Bulk-rock chromium contents can be related to the oxide and silicate fractions, with the latter influenced by terrestrial material.
- Uranium is bound to the silicate fraction and shows clear correlations with detrital elements implying anoxic conditions

## 1 INTRODUCTION

Iron formation (IF) deposition has been intrinsically linked to the oxygenation of Earth's near-surface environments (e.g. Ohmoto et al., 2006; Bekker et al., 2010; Konhauser et al., 2017), although the precise details of this complex relationship remain poorly understood. As chemical precipitates, both banded and granular iron formations can be used to reconstruct the composition of the oceans and atmosphere, using a variety of different techniques, proxies and models. Amongst these proxies are elemental abundances of various trace metals and their stable isotope ratios (e.g. Robbins et al., 2016).

Atmospheric oxygen on the early Earth was predominantly produced by oxygenic photosynthesis (e.g. Lyons et al., 2014). However, the timing of the onset of biological oxygen production and its relationship with Earth's first significant rise in atmospheric oxygen (the Great Oxidation Event (GOE)) at ca. 2.3 Ga remains enigmatic (e.g. Canfield, 2005; Buick, 2008). Various redox-sensitive isotope systems have been used to argue for an early onset of oxygenic photosynthesis, as much as a billion years prior to the GOE, including Mo-isotopes (e.g. Planavsky et al., 2014), Fe-isotopes (e.g. Dauphas et al., 2004) and Cr-isotopes (Crowe et al., 2013). Based on decreasing molar Ni/Fe ratios in IFs through time, Konhauser et al. (2009) proposed that methanogenesis decreased as a result of declining volcanic Ni inputs to seawater, so facilitating a rise in atmospheric oxygen as methane (an important sink for photosynthetic oxygen) was depleted. However, the only direct proxy to put a constraint on Archean atmospheric O<sub>2</sub> concentrations has been the disappearance of mass-independent fractionation of S-isotopes (Farquhar et al., 2000; Bekker et al., 2004; Guo et al., 2009; Luo et al., 2016). Beyond this, the GOE has been recorded in the Cu-isotope record of marine black shales (Chi Fru et al., 2016), the Zn/Fe ratio of marine carbonates (Liu et al., 2016), Co abundance in marine sediments (Swanner et al., 2014) and the appearance of Ce-anomalies in sediments (e.g. Bau and Dulski, 1996). Proxies for oxidative weathering in the Archean prior to the GOE include Mo concentrations and Re/Mo ratios in marine shales (Anbar et al., 2007; Kendall et al., 2010), U concentrations (Partin et al., 2013) and Cr-isotopes in IFs (Frei et al., 2011; 2016; Crowe et al., 2013). As well as their role as redox-indicators, various other trace elements in IF have been utilized to determine the input of allochthonous material, either detrital or volcanic ash. These trace elements are immobile in aqueous solutions and therefore can be used to

represent clastic input. Commonly used trace elements to check for clastic-contaminated IF-samples are Sc, Ti and Zr (e.g. Bau, 1993; Pecoits et al., 2009).

Iron formations are composite rocks containing three major Fe-bearing fractions; Fe-carbonates, Fe-oxides and Fe-silicates of a very fine-grained textural nature, which poses significant challenges for geochemical research. Physical separation of individual minerals in IF is practically unattainable. Therefore, bulk-rock analyses have been predominantly applied to IF samples to date (e.g. Johnson et al., 2003; Anbar, 2004; Rouxel et al., 2005; Yamaguchi et al., 2005; Tsikos et al., 2010; Planavsky et al., 2012). Bulk-rock data potentially reflect differences in modal mineralogy, as Fe-carbonates (e.g. siderite) tend to record lower  $\delta^{56}\text{Fe}$  values compared to coexisting Fe-oxides such as magnetite (e.g. Johnson et al., 2003, 2008a; Steinhoefel et al., 2009; 2010). Furthermore, even minor amounts of detrital materials can alter the geochemical bulk-rock signal significantly for minor and trace elements (e.g. Viehmann et al., 2015). Some studies have focussed on mono-mineralogical bands (siderite or magnetite) where possible (Johnson et al., 2008a; Heimann et al., 2010; Craddock and Dauphas, 2011) or single mineral grains (if large enough) using femto-second laser ablation inductively coupled plasma mass spectrometry (e.g. Steinhoefel et al., 2009; 2010). However, the mono-mineralogical band and micro-analytical techniques focus on small-scale variations that might be unsuitable for the elucidation of broader-scale trends across time and/or space. Furthermore, most bands in IFs are not mono-mineralogical and the very fine-grained nature makes micro-analytical techniques potentially biased towards larger grains.

Chemical separation of IF samples into different mineralogical fractions has the clear potential to allow the monitoring and evaluation of phase-specific effects on bulk-rock Fe-isotope values. Sequential extraction techniques use consecutive solvents, where each solvent dissolves a specific operationally-defined suite of minerals and has been widely developed for a variety of sample types and elements (e.g. Schilling et al., 2014; Siebert et al., 2015; Henkel et al., 2016). Multiple schemes have been developed using different solvents, varying reaction times and a wide range of sample types, including IFs (Poulton et al., 2004; Reinhard et al., 2009). This study builds on the sequential Fe extraction method developed by Poulton and Canfield (2005, hereafter referred to as P&C 2005). Here, the P&C 2005 protocol has been optimized for the very high Fe content in IF, and since there are only three key Fe-bearing mineral fractions, the number of different extracted fractions has been reduced. By varying the leaching times and conditions, using IF samples from the Transvaal Supergroup of South Africa with highly contrasting modal mineralogy, an optimum IF-extraction protocol has been obtained. This protocol was subsequently applied to >100 IF samples from the Transvaal Supergroup in order to study the speciation of various trace metals. Although trace metal isotope ratios are not explored here, the speciation of trace metals ultimately gives

insight into the applicability of sequential bulk-rock techniques for the stable isotope analysis of IF samples.

## **2 MATERIALS AND METHODS**

### **2.1 Sampling location and sample preparation**

The Asbestos Hills Subgroup in the Griqualand West section of the Transvaal Supergroup, South Africa, is dominated by two sequences of IF, the rhythmically micro-banded Kuruman IF Member and the overlying predominantly clastic-textured Griquatown IF Member (Beukes, 1984). These IFs were deposited immediately before the GOE around 2.52 to 2.43 Ga (Trendall et al., 1990; Sumner and Bowring, 1996; Pickard, 2003; Gumsley et al., 2017). Based upon sedimentological features, the Kuruman IF was deposited on an open-shelf environment below wave base, whereas the Griquatown Formation was deposited in a shallower marine environment (Beukes, 1984; Beukes and Klein, 1990). The IF horizons are interspersed with stilpnomelane lutite bands, which are considered to represent ash layers (Beukes, 1984). These iron formations were sampled from four diamond-drilled cores, originally obtained in the early 1990s during exploration for water resources by the mining industry: Gasesa-1, HEX-5, Erin-3 and Aarpan-5 (Figure 1). Samples were taken every 10-15 m core depth and consisted of 5-15 cm quarter-core fragments, capturing the diversity of IF in a total of 106 samples. Samples were crushed and then pulverized using a tungsten carbide swinging mill, followed by at least 30 minutes in an automated agate pulverisette to create a very fine-grained powder. Thin sections were made for each core piece. Bulk-rock sample characterization took place at Rhodes University, where the chemical composition was determined by XRF, and mineralogy was resolved by optical microscopy and XRD. Bulk-rock C and S concentrations were measured on a LECO CS-300 analyser and the minor and trace element chemistry was determined with a Thermo Scientific X-Series 2 ICP-MS after a standard bulk-rock digestion procedure using HF-HNO<sub>3</sub>-HClO<sub>4</sub> at Utrecht University.

### **2.2 Sample selection for assessment of sequential extraction methods**

The samples show a broad range in bulk-rock mineralogy and chemistry (full data tables given in supplementary material). Optical petrography in combination with XRD indicates the presence of the typical IF minerals in varying abundances. The carbonate minerals are dominated by ankerite and siderite in varying ratios with/without the presence of minor calcite. Magnetite is by far the dominant oxide mineral and hematite, if present at all, is a trace mineral in virtually all samples. Next to chert the silicate minerals greenalite, stilpnomelane, riebeckite and minnesotaite have also been found.

Three samples (HEX722, GAS488 and HEX836; Table 1), with highly contrasting mineralogical and chemical compositions, were selected for detailed sequential extraction analysis in order to optimize and revise previous Fe speciation protocols for IF. The carbonate-dominated HEX722-sample was taken from the upper part of the Griquatown Formation (Beukes, 1984) and consists of Fe-carbonate pelloids in a microcrystalline stilpnomelane/quartz matrix. Minnesotaite and calcite are also present in some pelloids. In thin section, magnetite appears only as a minor to trace mineral. Based on the XRD spectrum, siderite is the dominant carbonate, followed by ankerite and calcite in order of decreasing abundance. In contrast to sample HEX722, GAS488 is dominated by magnetite. This sample represents the rhythmically micro-banded Kuruman Formation, and is typified by alternating bands of microcrystalline quartz and magnetite (grain size up to 100  $\mu\text{m}$ ). At the edges of these bands, minute sub- $\mu\text{m}$  hematite grains are also present. Although peaks of carbonate minerals were not detected in the XRD spectrum, minor rhombohedral carbonates were observed in thin section. Dispersed riebeckite needles and stilpnomelane flakes were also identified microscopically but were undetectable in the XRD-spectra. Sample HEX836 consists of the three Fe-hosting mineralogical fractions in approximately equal proportions. The thin section reveals an alternation of stilpnomelane-magnetite-quartz, riebeckite-quartz and carbonate-dominated bands. XRD in conjunction with optical petrography revealed that the carbonate fraction is dominated by siderite in its typical very fine-grained rhombohedral habit (Figure S1).

The Fe-distribution of the first two samples is dominated by a single mineralogical fraction (Fe-carbonate or Fe-oxide). Consequently, the bulk of the Fe should be leached in a single chemical reaction step. In contrast to this, HEX836 consists of the three fractions in approximately even proportions and could therefore be used to further assess optimum geochemical leaching conditions. The certified reference material IF-G was also measured in duplicate using the final protocol, but was not a suitable rock type for testing the method due to the dominance of magnetite in the total Fe budget.

### **2.3 Sequential extraction schemes**

The sequential extraction scheme developed here is a modified version of the protocol designed by Poulton and Canfield (2005). The original protocol was developed to extract seven Fe phases, from “loosely sorbed” Fe to pyrite Fe, and calculated the unreactive silicate Fe by subtracting the sum of the extracted Fe from the bulk-rock Fe. The method has been successfully applied to both modern (e.g. März et al., 2008; 2012) and ancient Precambrian sediments (e.g. Poulton et al., 2004; Reinhard et al., 2009). In Precambrian sediments (shales and IF) only four phases are routinely extracted: carbonate-Fe, ferric oxide-Fe, magnetite-Fe and pyrite-Fe (Poulton et al., 2004; Reinhard et al., 2009).

Here we further optimized the P&C 2005-protocol for IFs which contain three Fe- phases: Fe-carbonates, magnetite and Fe-silicates. Sediment-sorbed Fe, ferrihydrite and goethite are not significant components of these 2.5 Ga rocks. Furthermore, the Asbestos Hills IFs are generally sulfur-poor ( $\ll 1$  wt%, Beukes and Klein, 1990), making the pyrite-Fe fraction negligible. The first two sequential extraction (SE) tests consisted of 4 original P&C 2005 steps used for Precambrian sediments and a final HF-HClO<sub>4</sub>-HNO<sub>3</sub>-step that was added to dissolve the silicate residue (Table 2). The dissolution of crystalline siderite in acetate might not be quantitative (Poulton and Canfield, 2005; Reinhard et al., 2009). This was assessed using the two different extraction conditions mentioned in P&C 2005; a 24 hr extraction at room temperature and a 48 hr extraction at 50 °C. To prevent contamination of the oxide fractions we included the original hydroxylamine-HCl step to collect any undissolved carbonate-Fe. Ideally we would combine the two subsequent oxide extractions into one leach, as hematite is only a trace constituent of the rocks and a clear separation of hematite from magnetite using the dithionite step might not be achieved (Henkel et al., 2016). In P&C 2005, NH<sub>4</sub>-oxalate was used to dissolve the magnetite, but it can also dissolve hematite (Suter et al., 1988; Panias et al., 1996; Taxiarchou et al., 1997). To confirm this we ran several tests with and without the dithionite step.

The setup of the six different SE-tests is presented in Table 3. The effectiveness of the different extractions was also tested with regard to atmospheric conditions. Several tests (SE1, 2, 4, 6) were performed under an inert N<sub>2</sub>-atmosphere, whereas the remaining (SE3, 5) were performed under an ambient atmosphere. The setup of a preliminary extraction (SE1) done in Cologne was run under similar conditions (SE2) in Utrecht, with the exception that the amount of reagents was increased from 5 to 10 ml. Sequential extraction 3 took place under an oxic atmosphere and the dithionite step was omitted. For the last three extraction tests (SE4-6), the acetate step was changed from 24 hours at 20 °C to 48 hours at 50 °C, following the recommendations by Poulton and Canfield (2005). With the exception of the acetate step conditions, SE4 was identical to SE2. SE5 and SE6 both omitted the hydroxylamine and dithionite steps. SE5 was performed under oxic and SE6 under inert conditions. The tests were performed in batches containing the test samples (GAS488 and HEX722) in triplicate as well as a blank and carbonatite standard, SARM-40 (Ring, 1993), in duplicate.

Following these tests, the optimum durations for the acetate and oxalate steps were tested using either the carbonate- or oxide-rich sample, respectively. The acetate step (SE-Ac) was performed under oxic conditions at 50 °C for 7, 24, 48 and 72 hours, followed by the 6-hour oxalate leach and the silicate digestion. For the oxalate step (SE-Ox) the extraction was tested, following the 48 hour, 50 °C acetate leach, at 6 and 24 hours for both atmospheric conditions. One extraction was completed in darkness and one was performed at 50 °C. These optimization tests included a duplicate sample (HEX722 for acetate and GAS488 for oxalate) and a control sample for each of the

conditions tested. These tests resulted in a working three-step sequential extraction protocol which could be applied to all samples.

## 2.4 Sequential extraction methodology

For each extraction step, the extracting reagent was pipetted into a 15 ml Greiner® tube containing ca. 50 mg of homogenized sample. The tubes were placed horizontally on a shaker (150 rpm) for the indicated reaction time. In case of extractions at elevated temperatures, a shaking incubator was used. After centrifuging (2500G, 15 min), the supernatants were syringe-filtered (0.45 µm), transferred to another 15 ml Greiner® tube and stored in a fridge at 5 °C. Due to extremely high Fe concentrations in the samples, the residue was always washed with MilliQ® water, centrifuged and decanted before the next reagent was added. Addition of extracting solutions and filtrations was performed in a N<sub>2</sub>-filled glove bag where indicated ('inert conditions', Table 3).

After the oxalate extraction, the residue was transferred with several rinses of MilliQ® from the Greiner® tube to a 30 ml Savillex® PFA-vial. After evaporation, 5.0 ml HF-HClO<sub>4</sub>-HNO<sub>3</sub> (5:3:2) were added to the vial to dissolve the residue overnight at 90 °C. This dissolution was followed by an evaporation step, after which the sample was re-dissolved in 10 ml 1.0 M HNO<sub>3</sub>. The solution was then transferred to a 15 ml Greiner® tube, and also stored in the fridge. After these optimization extractions the solutions were analysed for major elements by ICP-OES.

## 2.5 Analytical Techniques

Chemical separation of the samples was done in batches of 17-18 samples including one blank, two monitoring (GAS488 and HEX836) and two duplicate samples. Major and minor elements were determined using a Spectro Arcos ICP-OES and trace elements using a Thermo Scientific X-series 2 ICP-MS at Utrecht University. For ICP-MS analysis, a 10 µg/kg In-spike was used as an internal standard and quality control (QC) and drift checks were run every 6 samples. The low trace element concentrations encountered in IF forced the use of a lower than optimum dilution factor (10x instead of 50x). To counteract any matrix effects and the low dilution factor both the standards and the independent QC were prepared 3 times to match either the acetate, oxalate and HNO<sub>3</sub> (after HF-extraction) matrix of the samples. Because the measured concentrations ranged over several orders of magnitude, the calibration curves were weighted (weighing factors of 1/concentration) to increase accuracy close to the detection limit. Blank values were negligible and below the detection limit for most elements. However, for some transition metals (e.g. Cr, Zn, Cu and to a lesser extent Ni) the average blank values were anomalous for the acetate extraction, indicating reagent contamination, calibration or interference problems. Various trace metals (incl. Cr) are difficult to measure on ICP-MS due to spectroscopic-interferences (e.g. Jarvis et al., 1992) and others are prone to

contamination in reagents or lab-environments (e.g. Zn). The average blank values for Cr, Zn, Cu and Ni could represent up to 30 % of the average measured concentration (1-2  $\mu\text{g}/\text{kg}$  range) in the samples. Furthermore, blank values for these elements varied unpredictably within a run. To account for this, fraction-average blank corrections were applied for all elements.

The results for the sequential extractions were compared to mineralogical data determined by *in situ* laser ablation ICP-MS (LA-ICP-MS). This was performed at Utrecht University with a 193 nm wavelength COMPex 102 ArF excimer laser ablation system (Lambda Physik, Göttingen, Germany) connected to an Element 2 sector field ICP-MS (Thermo Scientific, Bremen, Germany). The ICP-MS was operated in low resolution mode, and the laser with an energy density of  $10 \text{ J}/\text{cm}^2$  and a pulse repetition rate of 10 Hz. The laser crater diameter (80  $\mu\text{m}$ ) was relatively large but was optimized to give low detection limits and high analytical precision. Data reduction of laser ablation data was performed using the GLITTER software.

The goal of this study was to compare sequential extraction data for samples with highly contrasting mineralogies, for which a normalization factor was required. For the acetate fraction the major elements were converted to oxides (all Fe was assumed to be ferrous iron) and summed together with the bulk-rock carbon as  $\text{CO}_2$  in wt%. Normalizing to 100% enabled the comparison of carbonate-poor and carbonate-rich samples as well as mineral-specific literature data. A similar strategy was applied to the oxide fraction, with all Fe assumed to be hosted in magnetite ( $\text{Fe}_3\text{O}_4$ ). The remaining portion was the silicate fraction, which could not be calculated directly since  $\text{Na}_2\text{O}$  (carbonate extraction in Na-acetate) and  $\text{H}_2\text{O}$  were not measured and the oxidation state of Fe potentially varied. A complication for the silicate fraction was that all samples contained chert, with the result that the other minerals in the fraction were 'diluted' in various amounts with  $\text{SiO}_2$ . Fractions which were below 10 wt% of the total suffered from high degrees of uncertainty, as their measured trace element values were generally at or near the detection limit and the multiplication factor was high. These samples were not used further for interpretation.

### 3 SEQUENTIAL EXTRACTION OPTIMIZATION

The absolute recoveries calculated for each sequential extraction against the bulk-rock XRF data are within analytical uncertainty (>95 %) for the major elements. Full results for the individual extractions are given in the online supplementary material. In the following sections we report elemental distributions normalized to total recovery of that specific element, with percentages averaged over the duplicate or triplicate samples.

### 3.1 Acetate-extracted iron

Tests with sample HEX722 (SE1-3) reveal that a 24 hr acetate treatment at room temperature was not sufficient to completely extract carbonate-Fe from carbonate-rich IF samples, as demonstrated before by Poulton and Canfield (2005). In the absence of ferrihydrite, the measured Fe in the hydroxylamine-step could only be from carried-over carbonate. Based on SE1-SE4, approximately 90 % of the bulk-rock Fe appears to be carbonate-bound (Figure 2a). A near complete extraction was achieved with a 48 hr treatment at 50 °C as proposed for crystalline samples by Poulton and Canfield (2005). In these longer duration tests the Fe recovery increased to 80-85 %, but 5-10 % was still transferred to the subsequent step.

To evaluate whether extending the duration further would lead to the full carbonate-bound Fe extraction, the SE-Ac test was performed up to 72 hours (Figure 3). This test, under oxic conditions at 50 °C, showed that while Fe recovery remained similar (84 %), more Si was also extracted suggesting that silicates were partially digested. Since most samples are not as carbonate-rich as HEX722, a reaction time of 48 hours was adopted to prevent undesirable silicate dissolution. We suggest using smaller sample sizes (30 mg) for carbonate-dominated IF.

There was a small increase in Fe extracted (max. 5 %) when using an inert atmosphere compared to an oxic one (Figure 2a). The optimum acetate extraction adopted in the optimized protocol was thus for 48 hours at 50 °C under an inert atmosphere with sample sizes of 50 mg, which were decreased to 30 mg for carbonate-dominated samples.

### 3.2 Oxalate-extracted iron

The magnetite-rich GAS488-sample was used to optimize the oxalate extraction and test the necessity of the dithionite step. This sample contains negligible amounts of hematite but still approximately 20 % of the extracted Fe was present in the dithionite leach for SE1, 2 and 4. The amount of Fe in the dithionite leach indicated significant magnetite dissolution during the dithionite step. These values were much higher than initially suggested by Poulton and Canfield (2005), but match those found by Henkel et al. (2016). The dithionite leach was shown to be unnecessary for magnetite-rich, hematite-poor IFs, since the total amount of Fe leached by dithionite and oxalate did not exceed that of the oxalate treatment alone (Figure 2b). In case a sample contains minor amounts of hematite these will probably dissolve completely, although our oxalate leach was not optimized for hematite dissolution (Taxiarchou et al., 1997).

The amounts of Fe extracted during the oxalate leach of SE6 were lower than expected based on previous extractions. This extraction took place in the incubator at 30 °C and, as a consequence, in darkness whilst the previous extractions were performed in daylight. The effect of light on Fe dissolution was confirmed by the SE-Ox tests (Figure 3). The SE-Ox test also revealed that a leaching

duration of 24 instead of 6 hours increased the amount of extracted Fe without increasing the Si concentration. Furthermore, leaching under oxic atmosphere resulted in higher Fe dissolution compared to treatment under inert conditions.

The oxalate extraction at 50 °C increased the recovery from 79 % to 90 % of bulk-rock Fe, but it also almost doubled the amount of Si leached (from 2.5 % to 4.6 % in sample HEX836). Although for magnetite-dominated samples leaching at 50 °C is considered favourable, the silicate leaching poses a dilemma for samples of mixed mineralogy. There was no clear cut extraction possible, so in the optimized protocol the sample size was reduced to approximately 30 mg for samples with more than 40 wt% Fe (i.e. magnetite-rich samples) to achieve more complete dissolution at room temperature. Based on these results, the optimal extraction of the oxide fraction in magnetite-rich IF-samples should be performed at room temperature and under lighted and oxic conditions for 24 hours.

### 3.3 Distribution of other major elements

Various other major elements could be used in addition to Fe to help assess the quality of the extractions (Figure 4). Based on the different IF minerals, the only ones which incorporate Ca are the carbonates; ankerite, calcite and, to a lesser extent, siderite (Klein, 1974; Gole, 1980; Pecoits et al., 2009). Manganese has been shown to be incorporated preferentially into the carbonate fraction in the Transvaal IFs (Johnson et al., 2013; Kurzweil et al., 2016), although minor amounts can also be present in stilpnomelane that would influence the silicate fraction (Klein, 1974; Gole, 1980). The percentages of these elements increase with the extended duration and temperatures of the acetate step, similar to that of iron discussed above, indicating improved carbonate dissolution during the longer leaches. Magnesium is distributed between the carbonate and silicate minerals, depending on the mineralogy. For the carbonate-rich HEX722 sample, only a small part is hosted in the silicates (8-10 %). The decrease of Mg present in the leaches following the acetate step from 35 % to 6 % confirms that the 48 hr acetate extraction at 50 °C was more suitable than the shorter extraction to dissolve the carbonates quantitatively.

Ideally, Si should only be extracted in the HF step. However, during the HF treatment Si was lost as gaseous silica-tetrafluoride complexes and thus could not be measured. Subtraction of the measured Si in the other steps from the bulk-rock XRF value shows >96 % of the Si to be present in the HF fraction (Figure 4), implying that the silicates were practically unaffected by preceding reagents. This was confirmed by the virtual absence of Mg in the oxalate step of the magnetite-rich GAS488. The small amount of Mg in the carbonate-rich HEX722 can be explained by incomplete carbonate dissolution. A summary of the protocol is given in Figure 5 that shows optimized methods for magnetite-rich IF samples.

## 4 RESULTS

### 4.1 Sequential extraction data

The external reproducibility for the sequential extractions was based on multiple extractions of the same sample that were measured independently, including eight duplicate samples and two samples replicated nine times. The average relative standard deviation (RSD) was 10.9 % for the major elements determined by ICP-OES (Si, Fe, Mg, Mn, Ca, K), which reduced to 3.7 % when the respective element content was 1.0 wt% or higher, and increased to 13.3 % when it was <1.0 wt%. No systematic variation was found in the reproducibilities for the different fractions. For the ICP-MS data (Al, Sc, Ti, V, Cr, Mn, Co, Ni, Cu, Zn, Y, Zr, Mo, U) the average RSD was 22.5 %, which also varied with abundance. The average RSD of element concentrations >10 mg/kg was 10.8 %, which increased to 25.6 % for concentrations <10 mg/kg.

When recoveries (sum of extracted fractions vs. bulk-rock value) were calculated per sample and then averaged for all 106 samples, the values around the detection limit introduced a significant uncertainty. To counter-act this, the recoveries were calculated by using the slope of the regression line (forced through zero) in the summed extractions vs. bulk-rock value plots (Figure 6). This meant that the lower values had less influence on the average recovery. For the trace metals the recoveries were excellent (0.90-1.10) with slightly higher recoveries for Sc (1.22; Figure 6). The  $R^2$  values of the linear regression lines were >0.95 for all but Cu (0.79), Zn (0.86), Mo (0.87) and Sc (0.90).

The trace metals were found to be unevenly distributed over the three fractions (Table 4; full data tables in supplementary files). Since the total recoveries were excellent, the data was normalized to the summed totals. Titanium and Zr were dominantly bound to the silicate fraction, with 86% extracted during the HF-step. The majority of Mn was bound to carbonates, with 89% of the Mn extracted during the acetate leach. Preferential incorporation of Mn in carbonates was also previously found in the Koegas Formation (Johnson et al., 2013; Kurzweil et al., 2016). Based on the distribution of the other elements it became evident that the oxide fraction was relatively depleted in trace metals (Figure 7). In the carbonate fraction a clear negative correlation ( $R^2 = 0.91$ ) was present between Fe (10.0-37.1 wt%) and Ca (0.303-28.3 wt%), related to the relative amounts of ankerite versus siderite. Magnesium (0.716-6.30 wt%) was slightly more abundant than Mn (0.112-5.10 wt%). In the oxide fraction an anti-correlation ( $R^2 = 0.77$ ) between Mg (up to 4.76 wt%) and Fe (59.1-71.8 wt%) indicated mineralogical exchange. Trace elements were generally below 10 mg/kg in all fractions except for Ti and Cr.

## 4.2 Microanalytical data

The results of the LA-ICP-MS analyses are plotted in Figure 8 (data in supplementary files), together with the ranges of the chemically extracted, fraction normalized data. The microanalytical data overlie their respective fraction normalized concentration averages and ranges for all the accepted extractions (see section 2.5). The variation within the sequential extraction data was larger than the mineral trace element data, but they generally matched within an order of magnitude (Figure 8). However, for some of the trace metals the average extracted amounts in the carbonate fraction were higher than the microanalytical data (e.g. V, Cr, Co, Cu, Mo).

## 5 DISCUSSION

### 5.1 Limitations of the sequential extraction technique

The most critical aspect of any sequential extraction scheme is the complete dissolution of the targeted mineral fraction, leaving the other fractions unaffected. Using the single-mineral dominated samples, the different extraction combinations outlined above (SE1-6, SE-Ac, SE-Ox) were setup to test the boundary conditions of each leach. Incomplete extraction for these samples is undesirable, but almost unavoidable since increasing target fraction recoveries also increased the dissolution of neighbouring fractions. Consequently, a sequential extraction applied to samples dominated by a specific mineral group will most likely lead to contamination of the step following the dominated target fraction.

#### 5.1.1 Acetate extraction

An explanation for incomplete iron recoveries by acetate might be the re-precipitation of Fe-(hydr)oxides during the leach. Precipitation is enhanced by the presence of oxygen, since the soluble ferrous iron oxidizes to insoluble ferric iron. The latter precipitates would consequently be transferred to the next extraction step. The Fe-concentrations of the inert extractions were indeed slightly higher than their oxid counterparts (Figure 2), indicating re-precipitation, albeit at a relatively minimal level.

Siderite dissolution in Na-acetate with and without atmospheric oxygen was thermodynamically modelled using PHREEQC (version 2.18.5570; Parkhurst and Appelo, 1999) in combination with the minteq.v4 database included in the software-package. In this process, 50 mg of siderite was equilibrated with 10 ml 1 M Na and H-acetate at a fixed pH of 4.5 and temperature of 50 °C with and without the presence of 5 ml air (where the 21 % O<sub>2</sub> is the only reactive species). The model shows that precipitation of ferric Fe-(hydr)-oxides is thermodynamically favourable. Despite this, no visual evidence for precipitation was observed during the leaches.

For carbonate-rich samples or crystalline carbonate minerals, the acetate extraction might not quantitatively dissolve all Fe-carbonates (Reinhard et al., 2009). A 24 hr, 10 % HCl extraction at room temperature should quantitatively extract all the microcrystalline siderite and ankerite (Raiswell et al., 1994; 2011). However, this method has also been shown to extract several percent of the silicate and magnetite bound Fe (Raiswell et al., 1994) and can also extract trace amounts of phosphate minerals (Smith et al., 2008). Therefore this extraction was considered unsuitable for Fe-oxide-rich IF samples. Sample HEX722 is an exceptionally carbonate-rich sample and most bulk-rock IF samples have lower modal carbonate abundances. Therefore, we prefer the acetate leach since it leaves the oxide and silicate fractions intact. However, this means that for carbonate-rich samples, the Fe concentration in the step succeeding the acetate might be overestimated, due to transfer of undissolved/re-precipitated carbonate-bound iron. Another option could have been to repeat the extraction step for the carbonate-rich samples and then to combine the extracts. For consistency with the other samples we preferred to decrease the sample size of the carbonate-dominated samples.

### 5.1.2 Oxalate extraction

The dissolution of oxides in oxalate depends for major part on the pH and temperature of the solution (Taxiarchou et al., 1997; 1998). We worked with a constant pH (3.7) following the original protocol (Poulton and Canfield, 2005). For the increased temperature experiments (50 °C), the amount of Fe dissolved was higher, but as noted earlier unwelcome silicate dissolution was observed. The combined total Fe dissolved in the dithionite and oxalate extractions (i.e. SE1, 2 and 4) was generally lower than their counterparts which excluded the dithionite step (SE3, 5 and 6; Figure 2). This might be explained by promotion of Fe oxide dissolution in oxalate in the presence of  $\text{Fe}^{2+}_{(\text{aq})}$  (Suter et al., 1988; Pnias et al., 1996; Taxiarchou et al., 1997). If a part of the oxides was already removed by dithionite leaching, the reaction during oxalate treatment might not have been catalysed by Fe(II) and, accordingly, the magnetite dissolution may have been incomplete for those extractions.

For the dissolution of hematite in oxalate the atmosphere is important (Taxiarchou et al., 1997) since  $\text{Fe}^{2+}_{(\text{aq})}$  needs to be present to catalyse the reaction. The dissolution of hematite is therefore enhanced by an inert atmosphere (Taxiarchou et al., 1997). For magnetite it might be less important, since ferrous iron is present in the structure (Taxiarchou et al., 1997; 1998).

## 5.2 Validation of the sequential extractions

Normalizing sequential extraction data per fraction has the advantage of enabling direct comparisons with independent microanalytical techniques. The fractions are generally a mixture of different minerals whereas the EMP and LA-ICP-MS techniques focus on specific grains. If the end-

member compositions can be determined for the specific minerals the mineral-mixtures in the fractions should fall in-between the extremes.

### 5.2.1 Carbonate fraction

The different carbonate minerals were analysed by EMP in multiple samples from the ERI core (Rafuza, 2015). The average major element composition of these individual minerals brackets the acetate-extracted values as would be expected. The near-purity of the carbonate extraction was confirmed by the low abundances of Si, K and Al, with averages of 1.52, 0.544 and 0.082 wt% respectively, which indicates only very minor contamination by silicate minerals. The samples with relative high Al and K concentrations include the stilpnomelane lutite sample, indicating that minor stilpnomelane digestion occurred in these cases. The high Si numbers (up to 5.30 wt%) are unrelated to the lutites or to other elements and seem to occur randomly, implying digestion of SiO<sub>2</sub>. As microcrystalline quartz Si was not dissolved by the acetate extraction (Tessier et al., 1979) a possible explanation for the silica presence in the EMP data are micron-scale chert inclusions in the rhombohedral carbonates. EMP data of these carbonates have an average of 1.2 wt% SiO<sub>2</sub>, supporting this possibility (Rafuza, 2015). Furthermore, literature EMP data show averages of 2.5 and 3.3 wt% SiO<sub>2</sub> in siderite and ankerite respectively (Pecoits et al., 2009), which also shows that silicate inclusions can be present.

The LA-ICP-MS data of some trace metals are at the lower end of the extracted range (Figure 8). There are three potential explanations for this; 1) erroneous laser-ablation data, for example due to calibration errors or an incorrectly estimated internal standard, 2) the ablated grains were not completely representative, or 3) the extraction data were inaccurate. The internal standards used in LA-ICP-MS were FeO for siderite (49.53 wt%) and CaO for ankerite (27.55 wt%). Based on this the other major elements (except Si) fit within the expected mineralogical ranges. The relative high Si concentration indicates the presence of the quartz matrix, since other typical elements present in the Fe-silicate minerals (Al<sub>2</sub>O<sub>3</sub> and K<sub>2</sub>O) were well below 0.1 wt%. If the internal standards were inaccurate, a systematic offset would be expected for all elements of that specific analysis. This is not the case, and in fact for most elements, the correlation between the techniques is excellent.

The average process blank correction carried out for the ICP-MS measurements affected the transition metals most significantly. Process blank values for Cr, Zn and Cu were up to 30 % of the average measured values in the IF samples, making the uncertainties for these elements significant. These elements are already amongst the most difficult to measure by ICP-MS due to spectroscopic and non-spectroscopic interferences (Jarvis et al., 1992). However, if no blank correction was applied, the fraction normalized values would deviate even more from the in situ ones.

The carbonate extraction was designed to digest all carbonate minerals, including the very fine grained siderite matrix portion, whereas the laser ablation analyses could only be performed on large grains (>80  $\mu\text{m}$ ). These larger grains potentially differ geochemically from the finer precipitate, due to a different crystallization history. Siderite LA-ICP-MS data from the Dales Gorge IF has trace element ranges of 6-27 mg/kg Cr, 0.4-18 mg/kg Cu and 6-59 mg/kg Zn (Pecoits et al., 2009), that are higher than our LA-ICP-MS data but fall in the range of the extracted values.

### 5.2.2 Oxide fraction

A clean leach of pure magnetite should, after normalization, consist of 72.4 wt% Fe (100 wt%  $\text{Fe}_3\text{O}_4$ ). Microprobe analyses of magnetite in IF show generally pure Fe end-member compositions, with less than 0.1 wt% of other oxides present (Klein, 1974; Gole, 1980; Pecoits et al., 2009). The highest measured oxide after FeO and  $\text{SiO}_2$  in the LA-ICP-MS results is MgO with values up to 0.436 wt%. The majority of the oxalate normalized samples have Fe values above 70 wt% (median 70.4). The most common contamination can be seen in Si and Mg with median values of 0.771 and 0.413 wt% respectively. This indicates that the oxalate extraction was quite specific, but still dissolved a small quantity of silicates. Median Ca and Mn values were <0.05 wt%, suggesting that virtually no cross-contamination between oxides and carbonates took place. Most microanalytical mineral trace element data follow the range indicated by the extractions, although lower ablation values were recorded for Cu, Mo and Y. The latter can potentially be explained by the digestion of REY-bearing phosphate minerals in oxalate (Uusitalo and Tuhkanen, 2000; Smith et al., 2008). This could potentially affect the application of this method for REE analysis, not further explored in this study. Trace metal LA-ICP-MS data from the Hamersley IFs (Pecoits et al., 2009) shows values for Cu, Mo and Y which are in the same range as our sequential extraction data.

The very low concentrations of all minor and trace elements in unaltered IF magnetite has been described before (Nadoll et al., 2014; Chung et al., 2015). This is also holds for the Kuruman and Griquatown IFs. The oxide fraction, and the microanalyses of magnetite, yield concentrations that are low compared to the other fractions (Figure 7). An exception to this trend is V (and to a lesser extent Cr), which is most enriched in the oxide-fraction. This inter-fraction relationship is similar in the Dales Gorge IF (Pecoits et al., 2009) and the V ranges found here are similar to other IF magnetites (Nadoll et al., 2014; Chung et al., 2015).

### 5.2.3 Silicate fraction

Direct comparison of different silicate fractions with each other is difficult as variable amounts of chert are responsible for the range in Fe/Si ratios. The ratios of the calculated  $\text{Al}_2\text{O}_3$ , MgO and FeO contents can be compared to literature EMP data of the four main Fe-bearing silicate

minerals; greenalite, minnesotaite, riebeckite and stilpnomelane. The sequential extraction data are generally within the ranges of these minerals. However, two groups of samples plot outside the fields outer limits. Samples with significantly higher  $\text{Al}_2\text{O}_3/\text{FeO}$  ratios are the stilpnomelane lutites, which could potentially contain some biotite (Beukes and Klein, 1990). End-member greenalite does not contain any Mg, so samples with very low  $\text{MgO}/\text{FeO}$  ratios can be considered as almost pure Fe-greenalite. The other major elements in these samples ( $\text{Al}_2\text{O}_3$ , MnO and  $\text{K}_2\text{O}$ ) are also absent. Another explanation could be the transfer of oxide-bound Fe. However, these samples are not the ones with the highest fraction of oxide-bound Fe.

For most of the trace elements, the LA-ICP-MS mineral data is at the higher end of the range seen in the silicate extractions. Dilution of the concentrations in the extracted samples due to the presence of chert is the most obvious explanation. Zirconium is, as expected, only present in the silicate fraction (Figure 7). Zirconium can be used as an indicator for clastic input. Zirconium shows no correlation with Fe, indicating that the majority of iron bound to the silicates is not of detrital origin.

To summarize, it appears that the majority of the sequential extraction data agree well with the mineral data. Some trace metals of the carbonate fraction deviate slightly from the expected values based on LA-ICP-MS. The silicate fraction is the most difficult to interpret since multiple Fe-silicates minerals are generally present and cation substitution can extensively alter the mineral chemistry, making potential modal mineralogy calculations based on the major elements a first order estimate at best. The silicate fraction is also potentially influenced by detrital input. To overcome this issue, the sequential extraction technique could be applied to microdrilled samples from individual IF layers. However, in these instances the minimum sample sizes might be a limiting factor as 30-50 mg is required for our method, and bulk sample characterization is also desirable.

### 5.3 Trace elemental behaviour

As discussed above, the major elements behave as expected, with Si and Al plotting in the silicate corner. Calcium is bound to the carbonate minerals and Mg is divided between the silicate and carbonate fractions (Figure 7). Iron varies significantly from samples dominated by a single fraction to evenly mixed samples, as expected based on sampling strategy. Only a few minor and trace elements are predominately present in a single fraction, such as Mn in the carbonate fraction and Ti, Zr and U in the silicate fraction, so most are distributed over multiple phases (Figure 7). Amongst these elements is Sc, which can be used as a proxy for detrital input (e.g. Bau, 1993), and was therefore expected to plot in the silicate corner. The high recovery for Sc (1.22; Figure 6) and the unexpected presence in the carbonate fraction (Figure 7) is most likely related to a spectroscopic-interference of the carbonate-ions ( $^{13}\text{C}^{16}\text{O}_2^+$ ; Jochum et al., 2012) on  $^{45}\text{Sc}$ , for which no correction can

be applied because the carbonate content varies per sample. This interference could also explain the high Sc concentrations in the micro-analytical carbonate data (Figure 8).

Iron isotope ratios vary extensively between co-existing Fe-carbonates and Fe-oxides (e.g. Johnson et al., 2003; 2008b), which means that any bulk-rock Fe-isotope signature is at least partially related to the sample mineralogy. Therefore bulk-rock Fe-isotope ratios in IF should be interpreted carefully when discussing oxidation states of the surface environment. Other non-traditional stable isotopic systems which have been used to infer the relative oxygenation of the Earth include Cr (Frei et al., 2009; Konhauser et al., 2011; Crowe et al., 2013) and Mo (e.g. Czaja et al., 2012). Also the bulk-rock abundance of U in IF (Partin et al., 2013) has been used to infer oxygenic weathering. With the available speciation data, first-order suggestions can be made about the applicability of these proxies in IF systems and whether some basic assumptions need to be revisited.

### 5.3.1 Molybdenum

Molybdenum abundance and isotope ratios have been used to infer paleo-oxidation states (Anbar and Rouxel, 2007 and references therein). In the modern oceans Mo is the most abundant trace element, due to the highly conservative behaviour of the molybdate ion ( $\text{MoO}_4^{2-}$ ) under oxic conditions (e.g. Robbins et al., 2016). The long oceanic residence time homogenises the Mo abundance and its isotopic composition (Siebert et al., 2003). A long term homogeneous oceanic molybdate reservoir has also been inferred for the Neoproterozoic, where both Mo concentration and  $\delta^{98/95}\text{Mo}$  increase with time (Kurzweil et al., 2015).

Under euxinic conditions Mo is sequestered from seawater due to its reaction with  $\text{H}_2\text{S}$  to form particle-reactive thiomolybdates (e.g. Algeo and Lyons, 2006; Anbar and Rouxel, 2007). In sulfur-poor settings the adsorption of Mo onto Mn-oxide crusts represents the most important Mo sink (e.g. Bertine and Turekian, 1973; Arnold et al., 2004). This latter mechanism preferentially adsorbs lighter Mo isotopes (Siebert et al., 2003). Molybdenum isotopes can thus be used to argue for oxic versus euxinic conditions in ancient marine settings (e.g. Arnold et al., 2004).

The presence of a light Mo isotopic signal in pre-GOE rocks would then potentially indicate the presence of oxidized Mn-species in the original sediment (Planavsky et al., 2014; Kurzweil et al., 2016). The presence of free  $\text{O}_2$  in pre-GOE sedimentary environments has also been made using coupled Fe-Mo isotopes (Czaja et al., 2012), Re-Mo geochemistry (Anbar et al., 2007; Wille et al., 2007; Kendall et al., 2010), varying  $\delta^{98/95}\text{Mo}$  in microbial carbonates (Voegelin et al., 2010) and combined Mo-C-O isotopes (Kurzweil et al., 2015). As sulfide can quantitatively scavenge Mo, thereby reducing the residence time dramatically, varying  $\delta^{98/95}\text{Mo}$  in sulfur-rich shales can indicate changing inputs, which is potentially related to oxidative weathering of sulfide-minerals (Duan et al.,

2010). The combined result of the aforementioned studies gives a robust indication for pre-GOE oxygenic photosynthesis and the occasional atmospheric whiffs of O<sub>2</sub> (Anbar et al., 2007).

Due to the low (<1 mg/kg) contents of Mo in IFs (Pecoits et al., 2009; Kurzweil et al., 2016), most studies around the GOE have focussed to date on (black) shales and/or carbonates which have higher Mo contents (e.g. Duan et al., 2010; Czaja et al., 2012). The Mo contents in the bulk-rock IF samples here follow this trend with ranges from 0.178 to 2.39 mg/kg and an average of 0.827 mg/kg (see supplementary file, Table S1). The Mo and Mn abundances and speciation are not related in any way. Molybdenum is distributed over the three fractions (Figure 7) and does not show any stratigraphic relationship with the carbonates. In the studies of Planavsky et al. (2014) and Kurzweil et al. (2016), content relationships between Mn and Mo in IFs were also absent, but a negative relationship was found between MnO content and  $\delta^{98/95}\text{Mo}$  (Figure 9). As found before in the Koegas Subgroup (Johnson et al., 2013), Mn in the Asbestos Hills IFs is primarily bound to the carbonates, which means that the presence of Mn in the carbonate fraction strongly influences the  $\delta^{98/95}\text{Mo}$  values. This hints at the presence of Mn-oxyhydroxides onto which the <sup>95</sup>Mo is preferentially adsorbed compared to <sup>98</sup>Mo (Siebert et al., 2003), which may then be reduced by dissimilatory iron reduction to form Mn-bearing carbonates in the Koegas Subgroup.

Kurzweil et al. (2016) noted that in their samples Fe-oxides are subordinate to Fe-carbonates and Fe-silicates. In our sequential extraction data Fe-oxides host similar amounts of Mo to the Fe-carbonates, even though Fe-oxides can adsorb significant amounts of Mo (e.g. Goldberg et al., 2009). Compared to the other fractions the Mo content in the silicate fraction is relative minor, and no relationship is seen between Zr and Mo suggesting no detrital control (Figure 10). Since the samples of Kurzweil et al. (2016) are carbonate and silicate dominated and if the silicate fraction does not contain significant Mo, as in our samples, then the MnO/ $\delta^{98/95}\text{Mo}$  relationship might be a function of oxide versus carbonate abundance instead of the presence of Mn-oxyhydroxides. In that case increased carbonate contents (MnO abundant) would have a low  $\delta^{98/95}\text{Mo}$  and oxide-rich samples a high  $\delta^{98/95}\text{Mo}$ .

The study by Planavsky et al. (2014) contains quantitative XRD data for a number of samples. The relative percentage of oxide minerals (hematite + magnetite) can be normalized to the sum of the oxides and carbonates (ankerite + siderite). When this percentage is plotted against the measured  $\delta^{98/95}\text{Mo}$  of the same samples two clear groups emerge. Carbonate dominated samples with  $\delta^{98/95}\text{Mo} < 0$  and positive  $\delta^{98/95}\text{Mo}$  for the oxide-rich samples (Figure 9). This alternative hypothesis might have some consequences for Mo isotope interpretation in IFs, and by extension shale samples. A quick way to test this would be to either measure bulk-rock Mo isotopes from the same sample set in this study, or to do Mo speciation on the samples by Kurzweil et al. (2016).

Fraction specific Mo isotopes will also improve our understanding, but this would be challenging to achieve.

### 5.3.2 Chromium

Chromium is a redox proxy that can be affected by a strong detrital influence (Tribovillard et al., 2006) and its supply to the modern oceans is therefore dominated by terrestrial processes (Konhauser et al., 2011). Chromium isotope fractionation has been used to infer the onset of oxidative weathering (Frei et al., 2009; Crowe et al., 2013), as conversion of insoluble trivalent to mobile hexavalent Cr preferentially releases the heavier  $^{53}\text{Cr}$  isotope. The product chromate ions can be readily reduced to Cr(III) in the presence of ferrous ions, of which the majority will hydrolyze to form insoluble  $\text{Cr}(\text{OH})_3$  (Reinhard et al., 2014) and co-precipitate with the ferric oxides. Because reduction of Cr(VI) by  $\text{Fe}^{2+}$  is efficient, the Cr residence time in the ferrous, anoxic Paleoproterozoic oceans would be very short, and the isotopic signature would be captured quantitatively (Frei et al., 2009).

Chromium isotopes have been used to argue for a very early (3.0 Ga) onset of oxygenic photosynthesis based upon fractionated values observed in a paleosol and a slightly younger iron formation (Crowe et al., 2013). Recent data from the Eoarchean IFs in Greenland indicate oxidative Cr cycling by 3.8 Ga (Frei et al., 2016), without necessarily needing the presence of cyanobacteria. The largest Cr isotope fractionations occur at the end of the Neoproterozoic coinciding with the diversification of eukaryotes and the rise of animals (Frei et al., 2009; Cole et al., 2016). This was preceded by minimal Cr oxidation throughout the mid-Proterozoic.

Cr abundances are dominated by detrital fluxes. By dividing Cr by Ti and then normalizing to the restoration model for the upper continental crust (values from Condie, 1993), authigenic Cr enrichment can be calculated for bulk-rock samples (Konhauser et al., 2011). This eliminates the variability in detrital input. The largest crustal normalized Cr/Ti ratios are observed in IFs coinciding with the GOE. This was explained by oxidative weathering of sulfides, causing acidity which would have enhanced *in situ* dissolution of Cr-bearing minerals (Konhauser et al., 2011). Such a model would also explain why the bulk-rock IF  $\delta^{53}\text{Cr}$  record does not vary extensively until the Neoproterozoic. The *in situ* dissolution does not include a Cr-fractionation step as Cr(III) does not necessarily need to be oxidized to Cr(VI). The minor fractionations seen before the GOE (Frei et al., 2009; 2016; Crowe et al., 2013) might also be related to such processes.

The lutite samples in the Asbestos Hills have a median Cr/Ti ratio of 0.033 which is nearly identical to the upper continental crustal ratio of 0.035 (Condie, 1993), which additionally supports their origin as volcanic ash layers (Table 5). The median bulk-rock Cr content of all 106 samples is 16 mg/kg, which is in the range for large-scale IFs (Konhauser et al., 2011). The median Cr/Ti ratio is

about three and nine times the crustal value for the Griquatown and Kuruman IFs respectively. The median Cr abundance increases from 11.5 to 16.3 mg/kg from the Kuruman to the Griquatown. The main factor in the changing ratio is the Ti concentration which increases from 32.1 to 124 mg/kg (Table 5). When looking at fraction specific level Cr and Ti behave opposite, the median Cr concentration tends to decrease from the acetate to the oxalate and HF leaches, whereas Ti increases. The HF Cr/Ti ratios are in good agreement with the upper continental crustal ratios (Table 5), indicating authigenic behaviour for the silicate bounded trace elements.

Although the uncertainties are significant, the fraction specific Cr concentration data for the carbonate fraction remain apparently homogeneous through the Asbestos Hills. For the oxide fraction there is a clear increase in Cr concentration from a 5.02 mg/kg median in the Kuruman Formation to 26.1 mg/kg in the Griquatown, which can be related to increased detrital input (as indicated by a correlation with Zr; Figure 10). This is also the case for the silicate fraction, although with slightly more scatter. This fits with the changing depositional environment as the Griquatown IF was deposited in shallower water, than the Kuruman Formation (Beukes, 1984; Beukes and Klein, 1990).

Instead of bulk-rock  $\delta^{53}\text{Cr}$ , carbonate-bound  $\delta^{53}\text{Cr}$  might be a more sensitive tracer for redox processes. A linear relationship was found between carbonate Cr concentration and  $\delta^{53}\text{Cr}$  in Ediacaran marine carbonates (Frei et al., 2011). Therefore carbonate-specific stable Cr isotopes could help to further construct the local redox conditions. However, in the Asbestos Hills, the virtually constant Cr concentration in the extracted carbonates might already indicate little  $\delta^{53}\text{Cr}$  variability at this time. The stratigraphically increasing Cr and Zr content in the oxide and silicate fraction indicate enhanced detrital input. This increase might potentially reflect increasing acid-weathering as suggested by Konhauser et al. (2011).

### 5.3.3 Uranium

Uranium concentrations (Partin et al., 2013; Satkoski et al., 2015), Th/U ratios (Bau and Alexander, 2009) and uranium isotope fractionation (Kendall et al., 2013) have been used to infer the presence of oxidative weathering. Sharing similarities with Cr, rock-hosted immobile U(IV) is oxidized to mobile U(VI) during this process. The seawater U budget is mainly controlled by riverine input, so increasing seawater U concentrations could indicate oxidative weathering (Partin et al., 2013). Once it reaches the Precambrian oceans U(VI) would be quantitatively trapped, either due to sorption onto ferric oxyhydroxides (Waite et al., 1994) and/or rapid reduction at an Fe-oxyhydroxide surface by Fe(II) and precipitation as a U(IV)-Fe(III) complex (Liger et al., 1999). However, U can also be brought in as a detrital uraninite grains (Johnson et al., 2014) under anoxic atmospheres.

The average measured U contents in the Kuruman and Griquatown IFs are low, at 0.047 and 0.082 mg/kg, respectively. The 5 lutite samples have an average at 1.45 mg/kg. When corrected for radioactive decay ( $U_{\text{corr.}} = U_{\text{measured}} \times e^{0.155125 \cdot \text{Age (Ga)}}$ ) in similar fashion as in Partin et al. (2013), these abundances become 0.07, 0.12 and 2.13 mg/kg, respectively. These values are more or less in line with the average, corrected U content in the Kuruman samples of 0.16 mg/kg (Klein and Beukes, 1989; Beukes and Klein, 1990; Bau and Dulski, 1996; Partin et al., 2013). The Asbestos Hills samples analysed by Horstmann and Hälbich (1995) and Pickard (2003) have a corrected average U content of 4.67 mg/kg, which is significantly higher than any sample measured in this study. The low U contents do not indicate an enhanced input through oxidative weathering in the Asbestos Hills IFs. This is confirmed by the strong relationships between bulk U content and Zr and Ti, with a  $R^2$  of 0.95 and 0.97, respectively (see supplementary file, Table S1). Furthermore, the majority of U is silicate hosted (ca. 70%; Figure 7), the U/Ti ratio remains constant throughout the stratigraphy, and the strong relationship with Zr (Figure 10) indicate a detrital or volcanic-ash origin for most of the U present. In addition, uraninite grains have not been found in the Asbestos Hills Subgroup, but the presence of them in the Koegas Subgroup (Johnson et al., 2014) supports this interpretation.

## 6 CONCLUSIONS

We have evaluated and adapted an existing sequential extraction procedure for sulfur-poor, magnetite-rich iron formation samples. The adaptation was necessary for two key reasons: to optimize previous methods for the very high FeO-content in IF samples (well over 50 wt% in many instances) and to reduce the number of different fractions used in the original scheme (Poulton and Canfield, 2005) to only the three key mineralogical fractions pertinent to the Asbestos Hills IF.

The final extraction scheme consists of three steps. Firstly, the micro-crystalline Fe-carbonates were dissolved in a pH 4.5 buffered 1.0 M Na-acetate solution, under an inert  $N_2$  atmosphere at 50 °C in a shaking incubator for 48 hours. Then, the Fe-oxides were digested using a 0.2 M ammonium oxalate/0.17 M oxalic acid solution for 24 hours at room temperature, under oxic and illuminated conditions. The final silicate residue was digested using a standard HF-HClO<sub>4</sub>-HNO<sub>3</sub> digestion protocol. Although optimized for IF samples, no clear-cut sequential extraction, with complete separation of the mineralogical components, was achieved. A balance was therefore sought between incomplete extraction and undesirable cross-dissolution of mineral components across subsequent fractions. For the final scheme, the elemental recoveries were good and the distribution of major elements (e.g. Mn, Ca, Mg and Si) showed no significant cross-contaminations. However, full dissolution of siderite or magnetite was impossible to check, since these fractions essentially contain only Fe and the Fe-distribution remains unknown.

Our optimized sequential extraction method was applied to 106 samples of the ca. 2.4 Ga IFs of the Kuruman and Griquatown Formations in the Griqualand West basin of the Transvaal Supergroup. Their deposition immediately prior to the Great Oxidation Event means that these IFs potentially capture the redox-changes in the surface environment on going from an anoxic to a sub-oxic atmosphere. The elemental concentrations in the various extracted fractions generally match the ranges found by microanalytical techniques on the individual minerals making up these fractions. Exceptions to this are some trace metals in the acetate fraction, such as Cr and Zn, which tend to be challenging to measure by ICP-MS. The distribution of most elements was found to be as anticipated, i.e. Al, Ti, Zr and U are mainly present in the silicate fraction, Mn and Ca are predominantly in the carbonate fraction, Mg is distributed among the silicates and carbonates and a few elements have a significant component bound to the Fe-oxides (Fe, Mo and V).

As suggested before for Fe, variable mineralogies with variable isotope ratios could compromise bulk-rock studies. This might also be the case for Mo and Cr, as they are distributed over multiple mineralogical phases. Bulk-rock concentration values for Cr and U do not hint to oxidative weathering at the time of IF deposition, which is consistent with their deposition in a practically detritus-free environment.

### **ACKNOWLEDGEMENTS**

We wish to thank ASSMANG Ltd for their generous funding and support towards the establishment of research unit PRIMOR at Rhodes University, under the umbrella of which this study was carried out. We also thank SOUTH32 in Hotazel, specifically Mr T. Rabuda and EP Ferreira for permitting unconstrained access to the four drillcores used in our research. The research was also supported by the Netherlands Research Centre for Integrated Solid Earth Sciences (grant number 2.2.3) which covered the lab costs in Utrecht, the German Research Foundation (DFG grant number STA 936/5-1 and KA 2769/3-1) and SWP acknowledges support from a Royal Society Wolfson Research Merit Award. Helen de Waard, Ton Zalm and Goonie Marsh are gratefully thanked for their support in the lab and during the measurements. Finally, we thank A.J.B. Smith and S. Viehmann for their positive and constructive reviews.

## REFERENCES

- Algeo T. J. and Lyons T. W. (2006) Mo–total organic carbon covariation in modern anoxic marine environments: Implications for analysis of paleoredox and paleohydrographic conditions. *Paleoceanography* 21,
- Anbar A. D. (2004) Iron stable isotopes: beyond biosignatures. *Earth Planet. Sci. Lett.* 217, 223-236.
- Anbar A. D. and Rouxel O. (2007) Metal Stable Isotopes in Paleoceanography. *Annu. Rev. Earth Planet. Sci.* 35, 717-746.
- Arnold G. L., Anbar A. D., Barling J. and Lyons T. W. (2004) Molybdenum isotope evidence for widespread anoxia in mid-Proterozoic oceans. *Science* 304, 87-90.
- Bau M. (1993) Effects of syn- and post-depositional processes on the rare-earth element distribution in Precambrian iron-formations. *European Journal of Mineralogy* 5, 257-267.
- Bau M. and Dulski P. (1996) Distribution of yttrium and rare-earth elements in the Penge and Kuruman iron-formations, Transvaal Supergroup, South Africa. *Precambrian Res.* 79, 37-55.
- Bekker A., Holland H., Wang P., Rumble D., Stein H., Hannah J., Coetzee L. and Beukes N. (2004) Dating the rise of atmospheric oxygen. *Nature* 427, 117-120.
- Bekker A., Slack J. F., Planavsky N. J., Krapež B., Hofmann A., Konhauser K. O. and Rouxel O. J. (2010) Iron formation: the sedimentary product of a complex interplay among mantle, tectonic, oceanic, and biospheric processes. *Economic Geology* 105, 467-508.
- Bertine K. K. and Turekian K. K. (1973) Molybdenum in marine deposits. *Geochim. Cosmochim. Acta* 37, 1415-1434.
- Beukes N. J. (1984) Sedimentology of the Kuruman and Griquatown iron-formations, Transvaal supergroup, Griqualand West, South Africa. *Precambrian Res.* 24, 47-84.
- Beukes N. J. and Klein C. (1990) Geochemistry and sedimentology of a facies transition—from microbanded to granular iron-formation—in the early Proterozoic Transvaal Supergroup, South Africa. *Precambrian Res.* 47, 99-139.
- Buick R. (2008) When did oxygenic photosynthesis evolve? *Philos. Trans. R. Soc. Lond. B. Biol. Sci.* 363, 2731-2743.
- Canfield D. E. (2005) The early history of atmospheric oxygen: homage to Robert M. Garrels. *Annu. Rev. Earth Planet. Sci.* 33, 1-36.
- Chi Fru E., Rodriguez N. P., Partin C. A., Lalonde S. V., Andersson P., Weiss D. J., El Albani A., Rodushkin I. and Konhauser K. O. (2016) Cu isotopes in marine black shales record the Great Oxidation Event. *Proc. Natl. Acad. Sci. U.S.A.* 113, 4941-4946.

- Chung D., Zhou M., Gao J. and Chen W. T. (2015) In-situ LA-ICP-MS trace elemental analyses of magnetite: The late Palaeoproterozoic Sokoman Iron Formation in the Labrador Trough, Canada. *Ore Geology Reviews* 65, 917-928.
- Cole D. B., Reinhard C. T., Wang X., Gueguen B., Halverson G. P., Gibson T., Hodgskiss M. S., McKenzie N. R., Lyons T. W. and Planavsky N. J. (2016) A shale-hosted Cr isotope record of low atmospheric oxygen during the Proterozoic. *Geology*, 44, 555-558, .
- Condie K. C. (1993) Chemical composition and evolution of the upper continental crust: contrasting results from surface samples and shales. *Chem. Geol.* 104, 1-37.
- Craddock P. R. and Dauphas N. (2011) Iron and carbon isotope evidence for microbial iron respiration throughout the Archean. *Earth Planet. Sci. Lett.* 303, 121-132.
- Crowe S. A., Døssing L. N., Beukes N. J., Bau M., Kruger S. J., Frei R. and Canfield D. E. (2013) Atmospheric oxygenation three billion years ago. *Nature* 501, 535-538.
- Czaja A. D., Johnson C. M., Roden E. E., Beard B. L., Voegelin A. R., Nägler T. F., Beukes N. J. and Wille M. (2012) Evidence for free oxygen in the Neoproterozoic ocean based on coupled iron–molybdenum isotope fractionation. *Geochim. Cosmochim. Acta* 86, 118-137.
- Dauphas N., van Zuilen M., Wadhwa M., Davis A. M., Marty B. and Janney P. E. (2004) Clues from Fe isotope variations on the origin of early Archean BIFs from Greenland. *Science* 306, 2077-2080.
- Duan Y., Anbar A. D., Arnold G. L., Lyons T. W., Gordon G. W. and Kendall B. (2010) Molybdenum isotope evidence for mild environmental oxygenation before the Great Oxidation Event. *Geochim. Cosmochim. Acta* 74, 6655-6668.
- Farquhar J., Bao H., and Thiemens M. (2000) Atmospheric influence of Earth's earliest sulfur cycle. *Science*, 289, 756-758.
- Frei R., Crowe S. A., Bau M., Polat A., Fowle D. A. and Døssing L. N. (2016) Oxidative elemental cycling under the low O<sub>2</sub> Eoarchean atmosphere. *Sci. Rep.* 6, 21058.
- Frei R., Gaucher C., Døssing L. N. and Sial A. N. (2011) Chromium isotopes in carbonates—a tracer for climate change and for reconstructing the redox state of ancient seawater. *Earth Planet. Sci. Lett.* 312, 114-125.
- Frei R., Gaucher C., Poulton S. W. and Canfield D. E. (2009) Fluctuations in Precambrian atmospheric oxygenation recorded by chromium isotopes. *Nature* 461, 250-253.
- Goldberg T., Archer C., Vance D., and Poulton, S. W. (2009) Mo isotope fractionation during adsorption to Fe (oxyhydr) oxides. *Geochim. Cosmochim. Acta*, 73(21), 6502-6516.
- Gole M. (1980) Mineralogy and petrology of very-low-metamorphic grade Archaean banded iron-formations, Weld Range, Western Australia. *Am. Mineral.* 65, 8-25.

- Gumsley A. P., Chamberlain K. R., Bleeker W., Soderlund U., de Kock M. O., Larsson E. R. and Bekker A. (2017) Timing and tempo of the Great Oxidation Event. *Proc. Natl. Acad. Sci. U. S. A.* 114, 1811-1816.
- Guo Q., Strauss H., Kaufman A. J., Schröder S., Gutzmer J., Wing B., Baker M. A., Bekker A., Jin Q., Kim S. T. and Farquhar J., (2009) Reconstructing Earth's surface oxidation across the Archean-Proterozoic transition. *Geology* 37, 399-402.
- Heimann A., Johnson C. M., Beard B. L., Valley J. W., Roden E. E., Spicuzza M. J. and Beukes N. J. (2010) Fe, C, and O isotope compositions of banded iron formation carbonates demonstrate a major role for dissimilatory iron reduction in ~ 2.5 Ga marine environments. *Earth Planet. Sci. Lett.* 294, 8-18.
- Henkel S., Kasten S., Poulton S. W. and Staubwasser M. (2016) Determination of the stable iron isotopic composition of sequentially leached iron phases in marine sediments. *Chem. Geol.* 421, 93-102.
- Horstmann U. E. and Hälbig I. W. (1995) Chemical composition of banded iron-formations of the Griqualand West Sequence, Northern Cape Province, South Africa, in comparison with other Precambrian iron formations. *Precambrian Res.* 72, 109-145.
- Jarvis K. E., Gray A. L. and Houk R. S. (1992) *Handbook of inductively coupled plasma mass spectrometry.* Blackie; Chapman and Hall, 256p.
- Jochum K. P., Scholz D., Stoll B., Weis U., Wilson S. A., Yang Q., Schwalb A., Börner N., Jacob D. E. and Andreae M. O. (2012) Accurate trace element analysis of speleothems and biogenic calcium carbonates by LA-ICP-MS. *Chem. Geol.* 318, 31-44.
- Johnson C. M., Beard B. L. and Roden E. E. (2008b) The iron isotope fingerprints of redox and biogeochemical cycling in modern and ancient Earth. *Annu. Rev. Earth Planet. Sci.* 36, 457-493.
- Johnson C. M., Beard B. L., Beukes N. J., Klein C. and O'Leary J. M. (2003) Ancient geochemical cycling in the Earth as inferred from Fe isotope studies of banded iron formations from the Transvaal Craton. *Contributions to Mineralogy and Petrology* 144, 523-547.
- Johnson C. M., Beard B. L., Klein C., Beukes N. J. and Roden E. E. (2008a) Iron isotopes constrain biologic and abiologic processes in banded iron formation genesis. *Geochim. Cosmochim. Acta* 72, 151-169.
- Johnson J. E., Gerpheide A., Lamb M. P. and Fischer W. W. (2014) O<sub>2</sub> constraints from Paleoproterozoic detrital pyrite and uraninite. *Geological Society of America Bulletin* 126, 813-830.

- Johnson J. E., Webb S. M., Thomas K., Ono S., Kirschvink J. L. and Fischer W. W. (2013) Manganese-oxidizing photosynthesis before the rise of cyanobacteria. *Proc. Natl. Acad. Sci. U. S. A.* 110, 11238-11243.
- Kendall B., Brennecke G. A., Weyer S., and Anbar A. D. (2013) Uranium isotope fractionation suggests oxidative uranium mobilization at 2.50 Ga. *Chemical Geology*, 362, 105-114.
- Kendall B., Reinhard C. T., Lyons T. W., Kaufman A. J., Poulton S. W. and Anbar A. D. (2010) Pervasive oxygenation along late Archaean ocean margins. *Nature Geoscience* 3, 647-652.
- Klein C. (1974) Greenalite, stilpnomelane, minnesotaite, crocidolite and carbonates in a very low-grade metamorphic Precambrian iron formation. *The Canadian Mineralogist* 12, 475-498.
- Klein C. and Beukes N. J. (1989) Geochemistry and sedimentology of a facies transition from limestone to iron-formation deposition in the early Proterozoic Transvaal Supergroup, South Africa. *Economic Geology* 84, 1733-1774.
- Konhauser K. O., Lalonde S. V., Planavsky N. J., Pecoits E., Lyons T. W., Mojzsis S. J., Rouxel O. J., Barley M. E., Rosière C. and Fralick P. W. (2011) Aerobic bacterial pyrite oxidation and acid rock drainage during the Great Oxidation Event. *Nature* 478, 369-373.
- Konhauser K. O., Pecoits E., Lalonde S. V., Papineau D., Nisbet E. G., Barley M. E., Arndt N. T., Zahnle K. and Kamber B. S. (2009) Oceanic nickel depletion and a methanogen famine before the Great Oxidation Event. *Nature* 458, 750-753.
- Konhauser K. O., Planavsky N. J., Hardisty D. S., Robbins L. J., Warchola T. J., Hugaard R., Lalonde S. V., Partin C. A., Oonk P. B. H., Tsikos H., Lyons T. W., Bekker A. and Johnson C. M. (2017) Iron Formations: A Record of Neoproterozoic to Paleoproterozoic Environmental History. *Earth Science Reviews* (accepted)
- Kurzweil F., Wille M., Gantert N., Beukes N. J. and Schoenberg R. (2016) Manganese oxide shuttling in pre-GOE oceans—evidence from molybdenum and iron isotopes. *Earth Planet. Sci. Lett.* 452, 69-78.
- Kurzweil F., Wille M., Schoenberg R., Taubald H. and Van Kranendonk M. J. (2015) Continuously increasing  $\delta^{98}\text{Mo}$  values in Neoproterozoic black shales and iron formations from the Hamersley Basin. *Geochim. Cosmochim. Acta* 164, 523-542.
- Liger E., Charlet L. and Van Cappellen P. (1999) Surface catalysis of uranium (VI) reduction by iron (II). *Geochim. Cosmochim. Acta* 63, 2939-2955.
- Liu X., Kah L., Knoll A., Cui H., Kaufman A., Shahar A. and Hazen R. (2016) Tracing Earth's O<sub>2</sub> evolution using Zn/Fe ratios in marine carbonates. *Geochemical Perspectives Letters* 2, 24-34.
- Luo G., Ono S., Beukes N. J., Wang D. T., Xie S. and Summons R. E., (2016) Rapid oxygenation of Earth's atmosphere 2.33 billion years ago. *Science advances* 2, e1600134.

- Lyons T. W., Reinhard C. T. and Planavsky N. J. (2014) The rise of oxygen in Earth's early ocean and atmosphere. *Nature* 506, 307-315.
- März C., Poulton S. W., Beckmann B., Küster K., Wagner T. and Kasten S. (2008) Redox sensitivity of P cycling during marine black shale formation: dynamics of sulfidic and anoxic, non-sulfidic bottom waters. *Geochim. Cosmochim. Acta* 72, 3703-3717.
- März C., Poulton S. W., Brumsack H. and Wagner T. (2012) Climate-controlled variability of iron deposition in the Central Arctic Ocean (southern Mendeleev Ridge) over the last 130,000 years. *Chem. Geol.* 330, 116-126.
- Nadoll P., Angerer T., Mauk J. L., French D. and Walshe J. (2014) The chemistry of hydrothermal magnetite: a review. *Ore Geology Reviews* 61, 1-32.
- Norrish K. and Hutton J. T. (1969) An accurate X-ray spectrographic method for the analysis of a wide range of geological samples. *Geochim. Cosmochim. Acta* 33, 431-453.
- Ohmoto H., Watanabe Y., Yamaguchi K. E., Naraoka H., Haruna M., Kakegawa T., Hayashi K. and Kato Y. (2006a) Chemical and biological evolution of early Earth: constraints from banded iron formations. *Geological Society of America Memoirs* 198, 291-331.
- Panias D., Taxiarchou M., Paspaliaris I. and Kontopoulos A. (1996) Mechanisms of dissolution of iron oxides in aqueous oxalic acid solutions. *Hydrometallurgy* 42, 257-265.
- Parkhurst D. L. and Appelo C. A. J. (1999) User's guide to PHREEQC (Version 2): A computer program for speciation, batch-reaction, one-dimensional transport, and inverse geochemical calculations. US Geological Survey, Water-Resources Investigations Report 99-4259, 312p.
- Partin C., Lalonde S. V., Planavsky N. J., Bekker A., Rouxel O., Lyons T. and Konhauser K. (2013) Uranium in iron formations and the rise of atmospheric oxygen. *Chem. Geol.* 362, 82-90.
- Pecoits E., Gingras M., Barley M., Kappler A., Posth N. and Konhauser K. (2009) Petrography and geochemistry of the Dales Gorge banded iron formation: Paragenetic sequence, source and implications for palaeo-ocean chemistry. *Precambrian Res.* 172, 163-187.
- Pickard A. (2003) SHRIMP U-Pb zircon ages for the Palaeoproterozoic Kuruman Iron Formation, Northern Cape Province, South Africa: evidence for simultaneous BIF deposition on Kaapvaal and Pilbara Cratons. *Precambrian Res.* 125, 275-315.
- Planavsky N. J., Asael D., Hofman A., Reinhard C. T., Lalonde S. V., Knudsen A., Wang X., Ossa F. O., Pecoits E., Smith A. J., Beukes N. J., Bekker A., Johnson T. M., Konhauser K. O., Lyons T. W., and Rouxel O. J. (2014) Evidence for oxygenic photosynthesis half a billion years before the Great Oxidation Event. *Nature Geoscience* 7, 283-286.
- Planavsky N. J., Rouxel O. J., Bekker A., Hofmann A., Little C. T. and Lyons T. W. (2012) Iron isotope composition of some Archean and Proterozoic iron formations. *Geochim. Cosmochim. Acta* 80, 158-169.

- Poulton S. W. and Canfield D. E. (2005) Development of a sequential extraction procedure for iron: implications for iron partitioning in continentally derived particulates. *Chem. Geol.* 214, 209-221.
- Poulton S. W., Fralick P. W. and Canfield D. E. (2004) The transition to a sulphidic ocean ~1.84 billion years ago. *Nature* 431, 173-177.
- Rafuza S. (2015) Carbonate Petrography and Geochemistry of BIF of the Transvaal Supergroup: evaluating the potential of Iron Carbonates as proxies for Palaeoproterozoic Ocean Chemistry. MSc thesis, Rhodes University, 105p
- Raiswell R., Canfield D. and Berner R. (1994) A comparison of iron extraction methods for the determination of degree of pyritisation and the recognition of iron-limited pyrite formation. *Chem. Geol.* 111, 101-110.
- Raiswell R., Reinhard C. T., Derkowski A., Owens J., Bottrell S. H., Anbar A. D. and Lyons T. W. (2011) Formation of syngenetic and early diagenetic iron minerals in the late Archean Mt. McRae Shale, Hamersley Basin, Australia: new insights on the patterns, controls and paleoenvironmental implications of authigenic mineral formation. *Geochim. Cosmochim. Acta* 75, 1072-1087.
- Reinhard C. T., Planavsky N. J., Wang X., Fischer W. W., Johnson T. M. and Lyons T. W. (2014) The isotopic composition of authigenic chromium in anoxic marine sediments: A case study from the Cariaco Basin. *Earth Planet. Sci. Lett.* 407, 9-18.
- Reinhard C. T., Raiswell R., Scott C., Anbar A. D. and Lyons T. W. (2009) A late Archean sulfidic sea stimulated by early oxidative weathering of the continents. *Science* 326, 713-716.
- Ring E. J. (1993) The Preparation and Certification of Fourteen South African Silicate Rocks for Use as Reference Materials\*. *Geostandards Newsletter* 17, 137-158.
- Robbins L. J., Lalonde S. V., Planavsky N. J., Partin C. A., Reinhard C. T., Kendall B., Scot, C., Hardisty D. S., Gill B. C., Alessi D. S. and Dupont C. L. (2016) Trace elements at the intersection of marine biological and geochemical evolution. *Earth-Science Reviews* 163, 323-348.
- Rouxel O. J., Bekker A. and Edwards K. J. (2005) Iron isotope constraints on the Archean and Paleoproterozoic ocean redox state. *Science* 307, 1088-1091.
- Satkoski A. M., Beukes N. J., Li W., Beard B. L. and Johnson C. M. (2015) A redox-stratified ocean 3.2 billion years ago. *Earth Planet. Sci. Lett.* 430, 43-53.
- Schilling K., Johnson T. M. and Mason P. R. D. (2014) A sequential extraction technique for mass-balanced stable selenium isotope analysis of soil samples. *Chem. Geol.* 381, 125-130.
- Schröder S., Bedorf D., Beukes N. J., and Gutzmer J. (2011). From BIF to red beds: Sedimentology and sequence stratigraphy of the Paleoproterozoic Koegas Subgroup (South Africa). *Sedimentary Geology*, 236, 25-44.

- Siebert C., Nagler T. F., von Blanckenburg F. and Kramers J. D. (2003) Molybdenum isotope records as a potential new proxy for paleoceanography. *Earth Planet. Sci. Lett.* 211, 159-171.
- Siebert C., Pett-Ridge J., Opfergelt S., Guicharnaud R., Halliday A. and Burton K. (2015) Molybdenum isotope fractionation in soils: Influence of redox conditions, organic matter, and atmospheric inputs. *Geochim. Cosmochim. Acta* 162, 1-24.
- Smith A. J. B., Gutzmer J., Beukes N. J., Reinke C. and Bau M. (2008) Rare Earth Elements (REE) in Banded Iron Formations - Link Between Geochemistry and Mineralogy. Ninth International Congress for Applied Mineralogy Proceedings, 651-658 (Australian Institute of Mining and Metallurgy: Carlton).
- Steinboefel G., Horn I. and von Blanckenburg F. (2009) Micro-scale tracing of Fe and Si isotope signatures in banded iron formation using femtosecond laser ablation. *Geochim. Cosmochim. Acta* 73, 5343-5360.
- Steinboefel G., von Blanckenburg F., Horn I., Konhauser K. O., Beukes N. J. and Gutzmer J. (2010) Deciphering formation processes of banded iron formations from the Transvaal and the Hamersley successions by combined Si and Fe isotope analysis using UV femtosecond laser ablation. *Geochim. Cosmochim. Acta* 74, 2677-2696.
- Sumner D. Y., and Bowring S. A. (1996) U-Pb geochronologic constraints on deposition of the Campbellrand Subgroup, Transvaal Supergroup, South Africa. *Precambrian Research*, 79, 25-35.
- Suter D., Siffert C., Sulzberger B. and Stumm W. (1988) Catalytic dissolution of iron (III)(hydr) oxides by oxalic acid in the presence of Fe (II). *Naturwissenschaften* 75, 571-573.
- Swanner E. D., Planavsky N. J., Lalonde S. V., Robbins L. J., Bekker A., Rouxel O. J., Saito M. A., Kappler A., Mojzsis S. J. and Konhauser K. O. (2014) Cobalt and marine redox evolution. *Earth Planet. Sci. Lett.* 390, 253-263.
- Taxiarchou M., Panias D., Douni I., Paspaliaris I. and Kontopoulos A. (1997) Dissolution of hematite in acidic oxalate solutions. *Hydrometallurgy* 44, 287-299.
- Taxiarchou M., Panias D., Douni I., Paspaliaris I. and Kontopoulos A. (1998) Dissolution of magnetite in acidic oxalate solutions. *Transactions of the Institution of Mining and Metallurgy-Section C-Mineral Processing* 107, 37-41.
- Tessier A., Campbell P. G. and Bisson M. (1979) Sequential extraction procedure for the speciation of particulate trace metals. *Anal. Chem.* 51, 844-851.
- Trendall A. F., Nelson D., Thorne A., Compston W., Williams I. and Armstrong R. (1990) Precise zircon U-Pb chronological comparison of the volcano-sedimentary sequences of the Kaapvaal and Pilbara cratons between about 3.1 and 2.4 Ga. In: Glover, J.E., Ho, S.E. (Eds.), *Proceedings of*

- the Third International Archaean Symposium, Perth, 1990, Extended Abstracts, pp. 81–83.  
Geoconferences (W.A.) Inc., Perth
- Tribovillard N., Algeo T. J., Lyons T. and Riboulleau A. (2006) Trace metals as paleoredox and paleoproductivity proxies: an update. *Chem. Geol.* 232, 12-32.
- Tsikos H., Matthews A., Erel Y. and Moore J. M. (2010) Iron isotopes constrain biogeochemical redox cycling of iron and manganese in a Palaeoproterozoic stratified basin. *Earth Planet. Sci. Lett.* 298, 125-134.
- Uusitalo R., & Tuhkanen H. R. (2000) Phosphorus saturation of Finnish soils: evaluating an easy oxalate extraction method. *Agric. Food Sci. Finland*, 9, 61-70.
- Viehmann S., Bau M., Hoffmann J. E. and Münker C. (2015) Geochemistry of the Krivoy Rog Banded Iron Formation, Ukraine, and the impact of peak episodes of increased global magmatic activity on the trace element composition of Precambrian seawater. *Precambrian Res.* 270, 165-180.
- Voegelin A. R., Nägler T. F., Beukes N. J. and Lacassie J. P. (2010) Molybdenum isotopes in late Archean carbonate rocks: implications for early Earth oxygenation. *Precambrian Res.* 182, 70-82.
- Waite T., Davis J., Payne T., Waychunas G. and Xu N. (1994) Uranium (VI) adsorption to ferrihydrite: Application of a surface complexation model. *Geochim. Cosmochim. Acta* 58, 5465-5478.
- Wille M., Kramers J., Nägler T. F., Beukes N. J., Schröder S., Meisel T., Lacassie J. and Voegelin A. (2007) Evidence for a gradual rise of oxygen between 2.6 and 2.5 Ga from Mo isotopes and Re-PGE signatures in shales. *Geochim. Cosmochim. Acta* 71, 2417-2435.
- Yamaguchi K. E., Johnson C. M., Beard B. L. and Ohmoto H. (2005) Biogeochemical cycling of iron in the Archean–Paleoproterozoic Earth: constraints from iron isotope variations in sedimentary rocks from the Kaapvaal and Pilbara Cratons. *Chem. Geol.* 218, 135-169.

**FIGURE CAPTIONS:**

Figure 1: Regional geology of the Griqualand West Basin in the Kaapvaal Craton (modified from Schröder et al., 2011) showing the locations of the drill cores selected for this study and their respective schematic logs. The small triangles indicate the sample depths of the in total 106 samples. The three yellow stars indicate the samples used to test the sequential extraction scheme (GAS488, HEX722 and HEX836).

Figure 2: Fe distribution results from the different tests for the samples HEX722 (a) and GAS488 (b).  $\Delta$  reagent is the difference between the amount of reagent used (SE1: 5 ml; rest 10 ml),  $\Delta$  atm is the difference between extraction under inert and oxic atmospheres,  $\Delta$  amount is the difference between 50 and 30 mg of sample used and  $\Delta$  light the light and dark conditions. See text for full discussion.

Figure 3: Fe distribution (normalized to total Fe extracted) for the SE-Ac and SE-Ox tests. The colours indicate the type of atmosphere and the durations for the extractions are mentioned. The inert samples (48 hr) in the acetate test are the results from SE6. For acetate tests, sample HEX722 was used. GAS488 was used for oxalate tests.

Figure 4: Elemental distribution among the five fractions for the different tests (averaged over triplicate samples), as percentages of total extracted. Silicon is quantitatively lost during HF-evaporation, so these percentages are based on bulk-rock values.

Figure 5: Block diagram showing the final sequential extraction procedure used to process all 106 IF samples.

Figure 6: Recoveries as slope of the regression line for the major elements and trace metals. A) Regression line slope versus the bulk-rock abundance (mg/kg). Regression lines for individual element Fe (B), Mn (C), Cr (D) and Co (E) analyses.

Figure 7: Averaged distribution of the major and trace elements over the three different fractions.

Figure 8: Sequentially extracted and LA-ICP-MS mineral specific trace element concentration ranges. Black lines are the sequentially extracted ranges per element for acetate, oxalate and HF from top to bottom, respectively. The three filled black diamonds are, from left to right, the 5<sup>th</sup> percentile, the

median and the 95<sup>th</sup> percentile of the range in the data. Overlain are the individual grain-specific analyses for the carbonates (blue), magnetite (red) and the Fe-silicate (green) minerals, with each symbol representing the average of 1-4 analysis sites in a thin section.

Figure 9: Bulk-rock MnO (wt%) versus Mo,  $\delta^{56}\text{Fe}$  and  $\delta^{98/95}\text{Mo}$  in IF samples and below the portion of oxide minerals present versus  $\delta^{98/95}\text{Mo}$ . Data from Planavsky et al. (2014), Kurzweil et al. (2016) and this study. Note the logarithmic MnO scale. See text for discussion.

Figure 10: Various trace metals (Cr, Mo, U) vs Zr for the bulk-rock and the three different fractions. Only accepted samples included. Where present, a positive linear trend indicates a correlation between the trace metal abundance and the presence of a detrital component. Note that the low Zr abundance in the carbonate fraction (<1 mg/kg), indicating no detrital component in this fraction. See text for discussion.

## TABLES:

Table 1: Bulk-rock compositions of the samples in wt%;  $\delta^{56}\text{Fe}$  in ‰ relative to IRMM-014. Typical external reproducibilities for  $\delta^{56}\text{Fe}$  were 0.1‰ (2SD)

	SiO <sub>2</sub>	Al <sub>2</sub> O <sub>3</sub>	FeO	MnO	MgO	CaO	K <sub>2</sub> O	LOI	Total	C	S	$\delta^{56}\text{Fe}$
<b>GAS488</b>	37.2	b.d.l.	52.9	0.05	2.10	0.83	b.d.l.	6.03	99.4	0.37	0.11	0.42
<b>HEX722</b>	22.4	0.51	32.7	4.91	4.34	4.76	0.28	29.16	99.6	7.92	0.20	-1.77
<b>HEX836</b>	38.2	0.34	40.1	0.27	4.82	0.31	1.04	14.31	99.7	3.18	0.12	-0.60

TiO<sub>2</sub>, P<sub>2</sub>O<sub>5</sub>, Na<sub>2</sub>O and H<sub>2</sub>O<sup>-</sup> < 0.1 wt%; All Fe as FeO; oxide data from XRF (b.d.l. = below detection limit), C and S from LECO CS

Table 2: Fractions and solvents used in this study and based on Poulton and Canfield (2005)

Target fraction	Solvent	Duration
Carbonates	1 M Na-acetate at pH 4.5 adjusted with acetic acid	24/48 hrs
Easily reducible oxides	1 M Hydroxylamine-HCl in 25% v/v acetic acid (pH 2.0)	48 hrs
Reducible Fe-oxides	50 g/L Na-dithionite buffered to pH 4.8 with 0.35 M acetic acid/0.02 M Na-citrate*	2 hrs
Magnetite	0.2 M ammonium oxalate/0.17 M oxalic acid solution (pH 3.7)	6 hrs
Silicates	5:3:2 v/v of HF (48%), HClO <sub>4</sub> (72%) and HNO <sub>3</sub> (65%) resp.	12 hrs

\* The P&C2005 protocol uses 0.2 M Na-citrate, here reduced to 0.02 M following Henkel, et al. (2016).

Table 3: Setup for extraction (SE) tests

	SE1	SE2	SE3	SE4	SE5	SE6
Where	Cologne	Utrecht	Utrecht	Utrecht	Utrecht	Utrecht
Atmosphere	Inert	Inert	Oxic	Inert	Oxic	Inert
Acetate	24 hr/20 °C	24 hr/20 °C	24 hr/20 °C	48 hr/50 °C	48 hr/50 °C	48 hr/50 °C
Hydroxylamine	Yes	Yes	Yes	Yes	-	-
Dithionite	Yes	Yes	-	Yes	-	-
Oxalate	Yes	Yes	Yes	Yes	Yes	Yes <sup>2</sup>
Hydrofluoric acid	Yes <sup>1</sup>	Yes	Yes	Yes	Yes	Yes

<sup>1</sup>HF-step performed at Utrecht University <sup>2</sup>Leached in darkness at 30 °C

Table 4: Fraction normalized concentration ranges with 5<sup>th</sup> percentile, average, 95<sup>th</sup> percentile and maximum values. Ca-Al in wt% and Sc-Mo in mg/kg. Only samples included when more than 10 wt% of the sample is the specific fraction.

	Carbonate fraction				Oxide fraction				Silicate fraction			
	5 <sup>th</sup>	Av.	95 <sup>th</sup>	Max.	5 <sup>th</sup>	Av.	95 <sup>th</sup>	Max.	5 <sup>th</sup>	Av.	95 <sup>th</sup>	Max.
Ca	0.679	7.74	18.2	28.3	0.018 2	0.043 6	0.085 9	0.110	0.005 43	0.147	0.515	1.67
Fe	15.2	27.5	36.3	37.2	61.2	69.0	71.6	71.8	2.74	12.4	23.8	31.8
Mg	2.15	3.70	4.85	6.30	0.051 5	0.886	3.27	4.76	0.100	0.947	2.24	2.80
Mn	0.199	1.41	3.84	5.1	0.003 44	0.095 6	0.335	0.628	0.002 54	0.045 5	0.137	0.342
Si	0.388	1.52	3.73	5.30	0.376	1.05	3.24	4.30	26.6	35.9	43.9	45.7
Al	0.006 64	0.072 6	0.217	1.12	0.006 93	0.196	0.633	2.37	0.012 8	0.371	1.33	4.54
Sc	0.531	2.66	6.96	19.7	0.105	0.927	3.50	6.35	0.054 4	0.685	2.57	7.23
Ti	0.560	4.47	11.0	17.8	11.1	144.	456.	656.	7.51	284.	1370.	2680.
V	1.55	7.56	23.3	49.1	4.05	17.3	40.9	112.	0.214	6.49	29.4	70.2
Cr	2.04	27.5	95.9	228.	0.985	21.3	74.3	126.	0.539	8.21	26.8	80.3
Co	0.555	2.34	6.08	17.1	0.109	1.92	3.71	58.6	0.121	1.84	7.68	9.75
Ni	2.24	9.45	27.5	66.4	0.710	6.45	17.2	26.6	0.677	5.27	16.7	45.2
Cu	2.63	15.2	36.0	67.5	2.12	8.29	15.3	24.0	0.928	5.59	16.6	23.1
Zn	2.48	13.3	34.3	70.5	0.699	5.74	16.9	27.9	0.535	6.42	15.1	61.3
Y	2.70	7.38	12.9	18.1	0.681	4.40	12.8	24.6	0.137	1.91	6.10	11.0
Zr	0.017 3	0.18	0.67	3.19	0.492	4.75	16.2	21.8	0.629	10.2	38.0	121.
Mo	0.287	1.36	3.78	13.8	0.596	1.80	4.09	7.11	0.076 3	0.342	0.989	2.36
U	0.010 9	0.107	0.425	1.10	0.003 84	0.068 2	0.229	0.465	0.001 90	0.159	0.601	2.39

Table 5: Cr and Ti behaviour through the sample set. Left side: median Cr and Ti concentrations of all samples. Right side median taken after ratios were calculated per sample, whereby n= gives the amount of Cr-Ti pairs used, so dividing the median Cr and Ti value does not necessarily result in the median Cr/Ti ratio. Abbreviations: BR = bulk-rock values, Ac. = Acetate fraction, Ox. = oxalate fraction, HF = HF fraction.

Fraction:		Median concentration (mg/kg)				Median Cr/Ti ratio				
		BR.	Ac.	Ox.	HF	BR.	Ac.	Ox.	HF	
Lutite	Cr	73.8	25.4	126.	75.5	Cr/Ti	0.033	1.433	0.192	0.028
	Ti	2120.	15.1	657.	2510.	n=	5	4	1	5
Griquatown	Cr	16.3	17.1	25.6	6.12	Cr/Ti	0.119	3.105	0.162	0.033
	Ti	124.	4.96	125.	169.	n=	67	48	38	65
Kuruman	Cr	11.5	23.6	5.02	1.19	Cr/Ti	0.332	5.429	0.087	0.041
	Ti	32.1	4.85	34.2	26.6	n=	34	17	15	27
All samples	Cr	15.7	19.9	16.7	4.87	Cr/Ti	0.149	3.168	0.158	0.034
	Ti	93.7	5.18	83.6	125.	n=	106	69	54	97

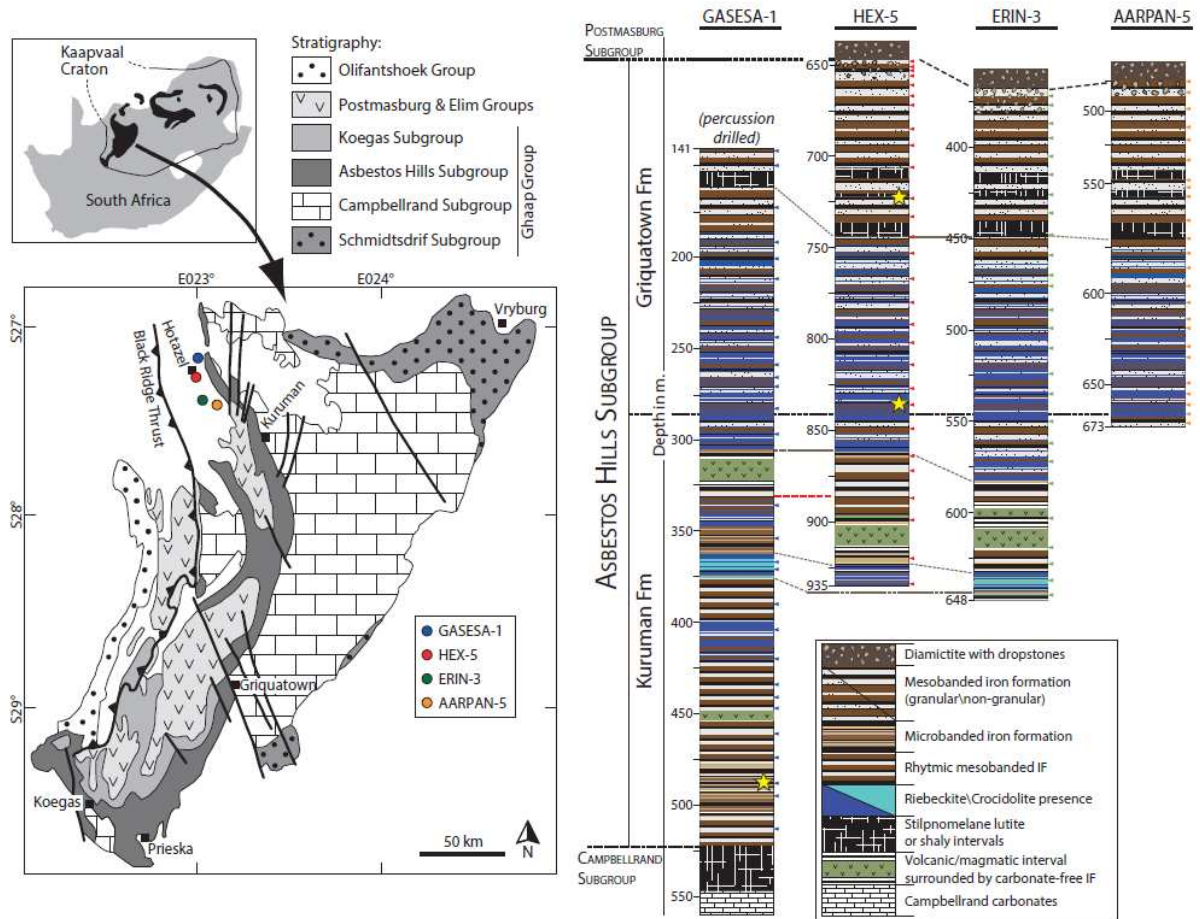


Fig. 1

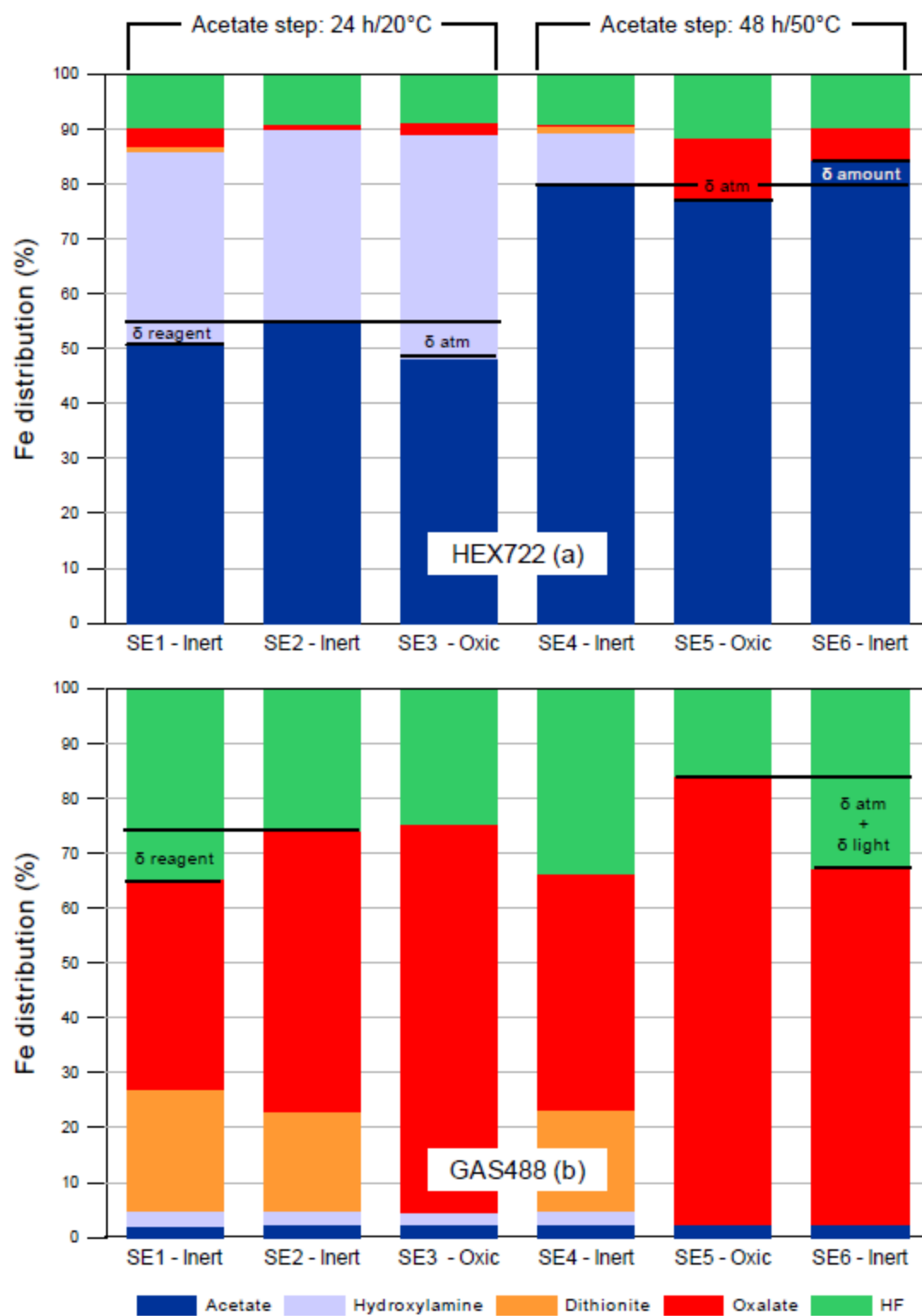
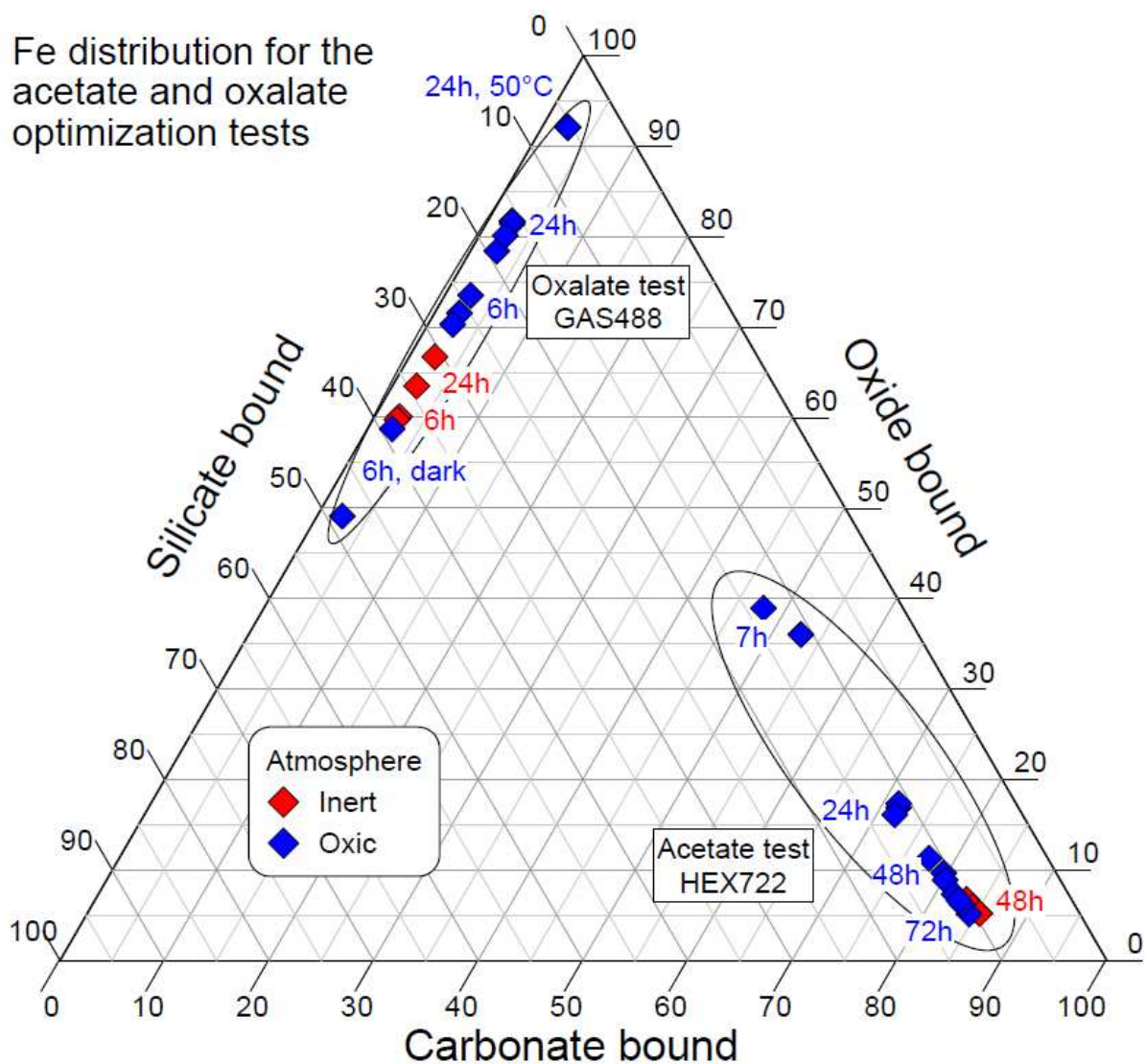


Fig. 2

Fe distribution for the acetate and oxalate optimization tests





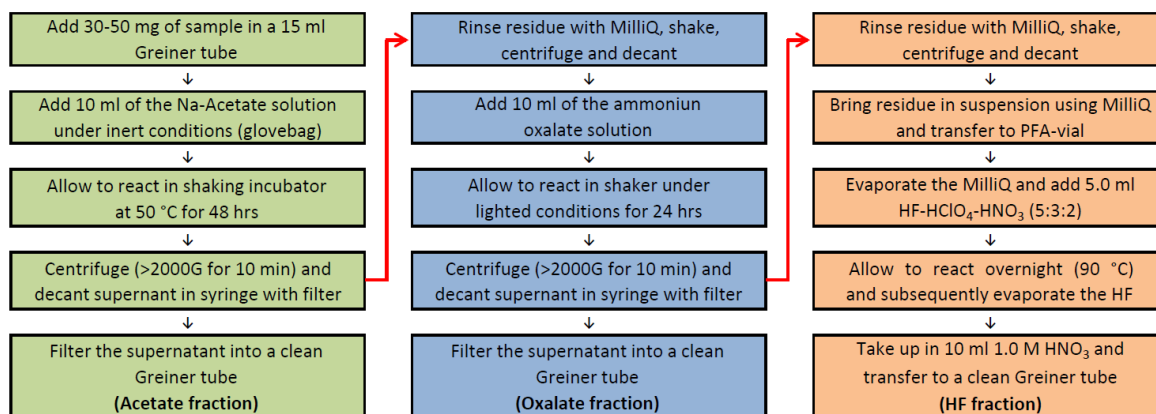


Fig. 5

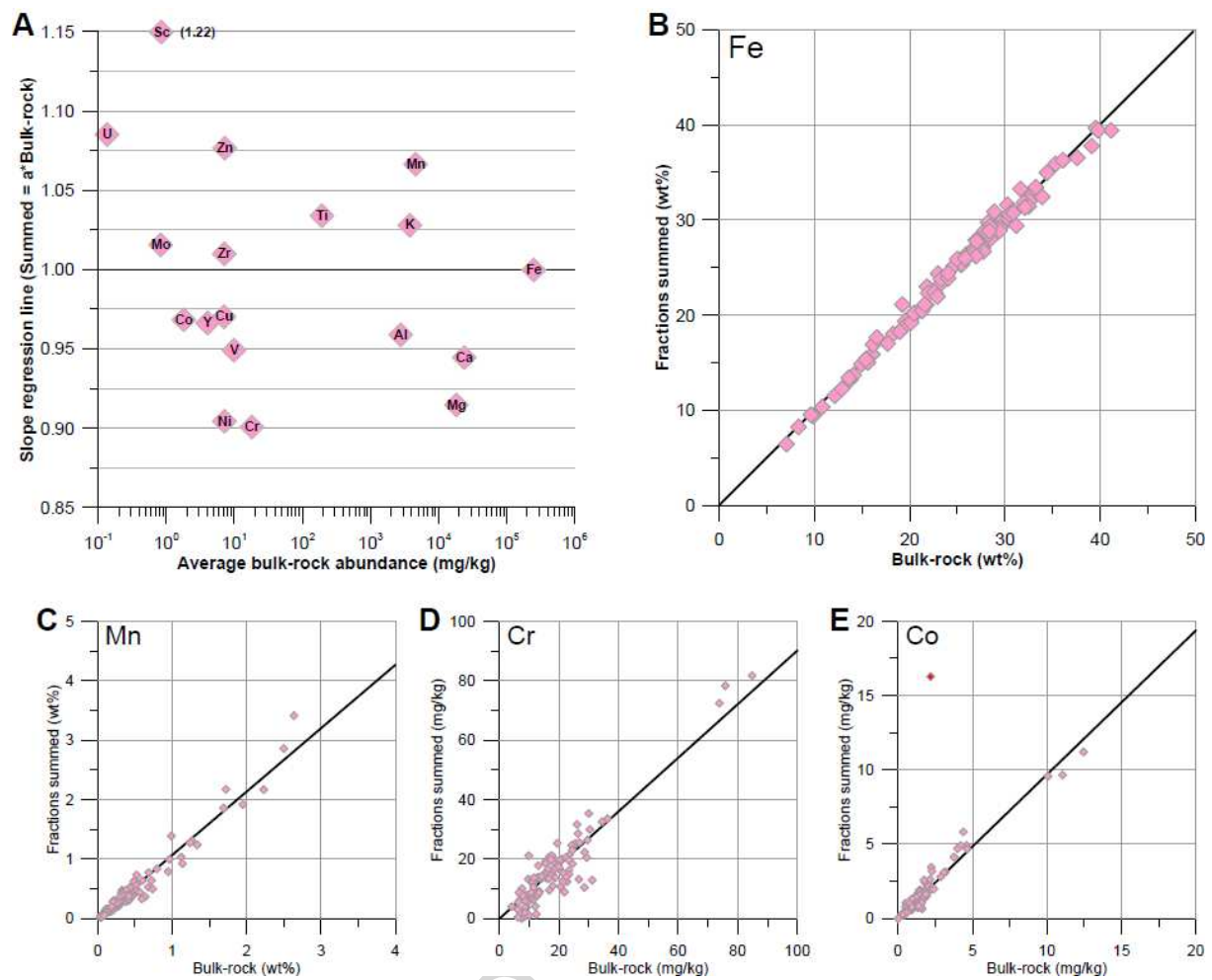


Fig. 6

## Averaged distribution

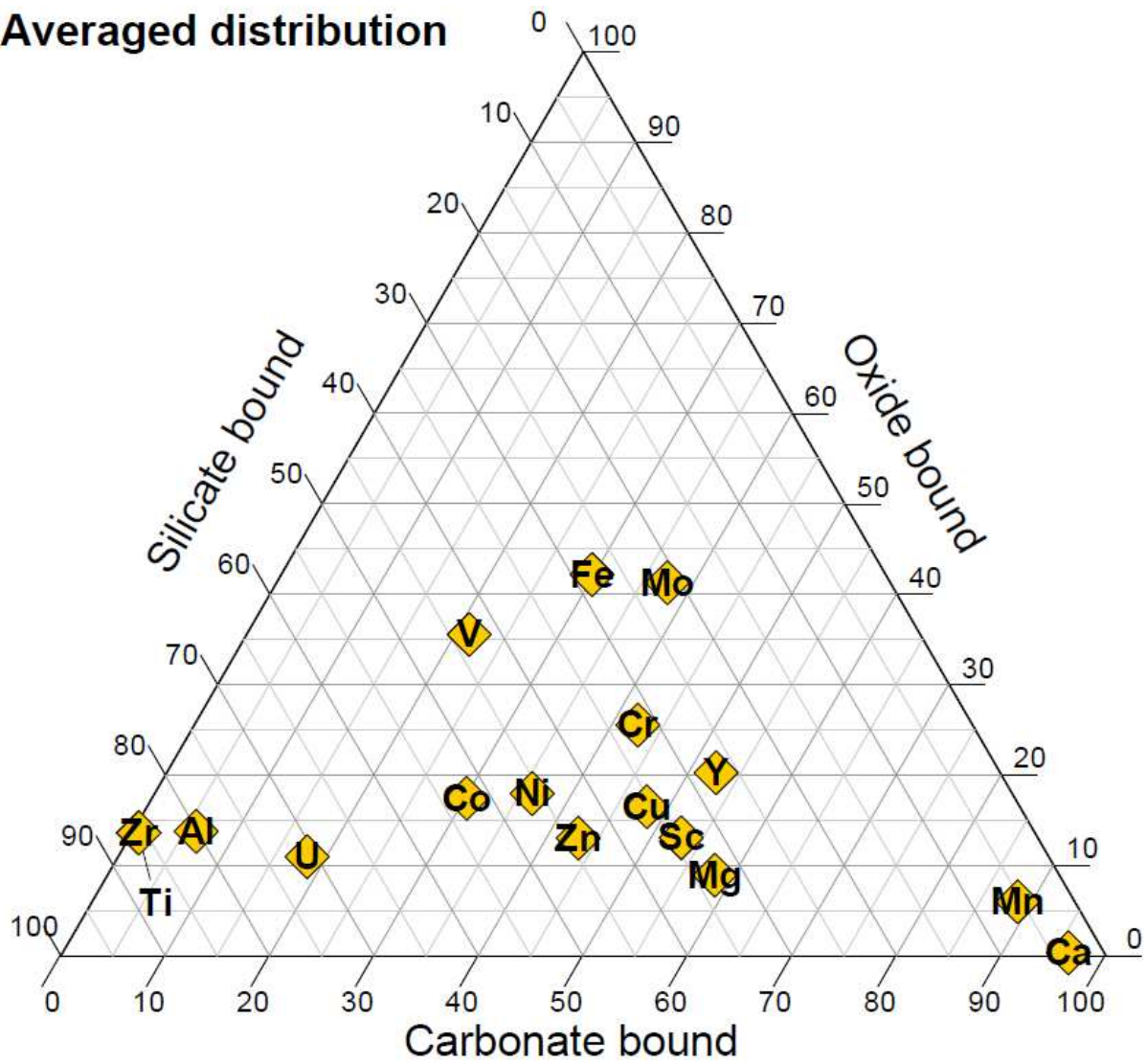


Fig. 7

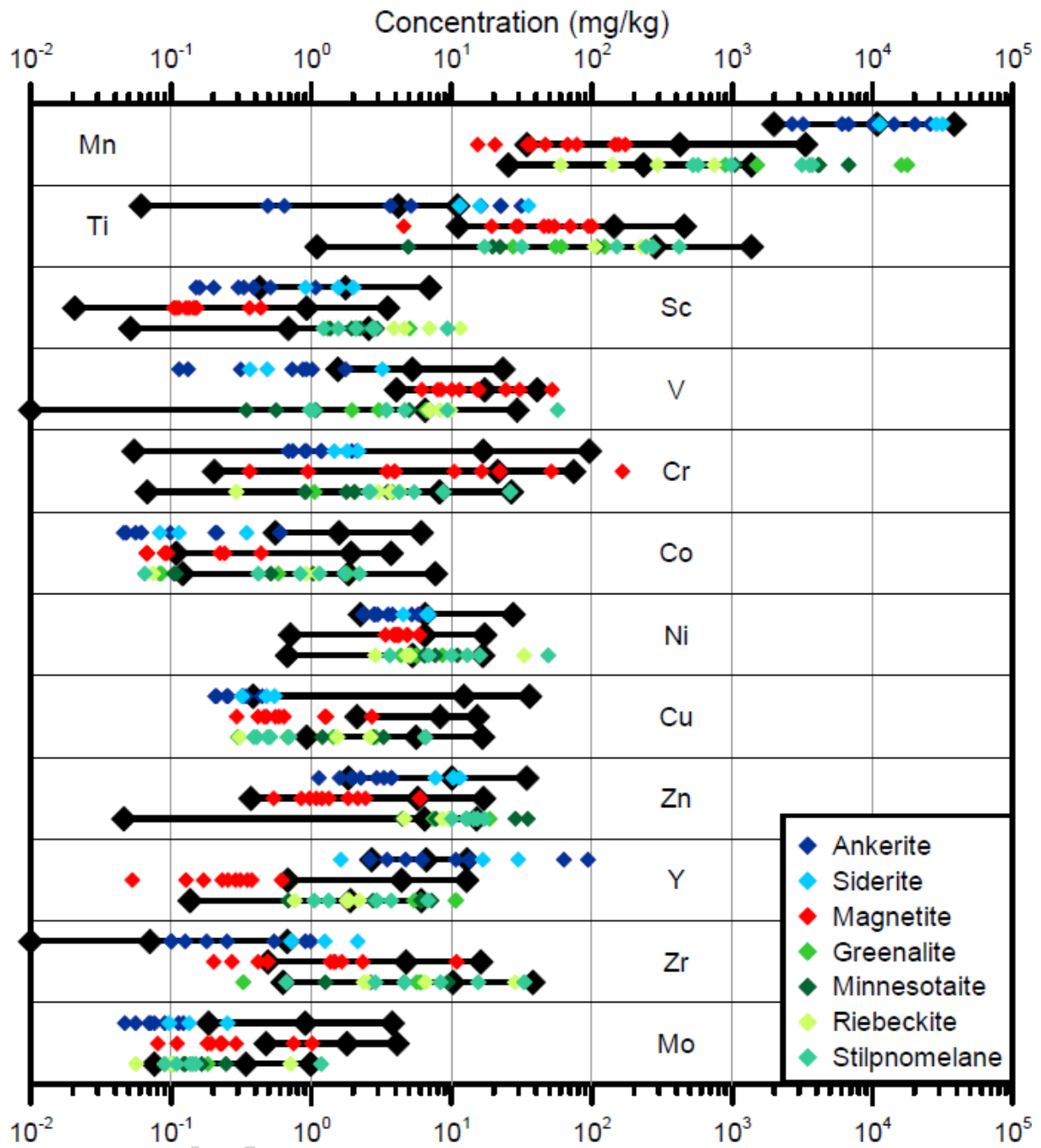


Fig. 8

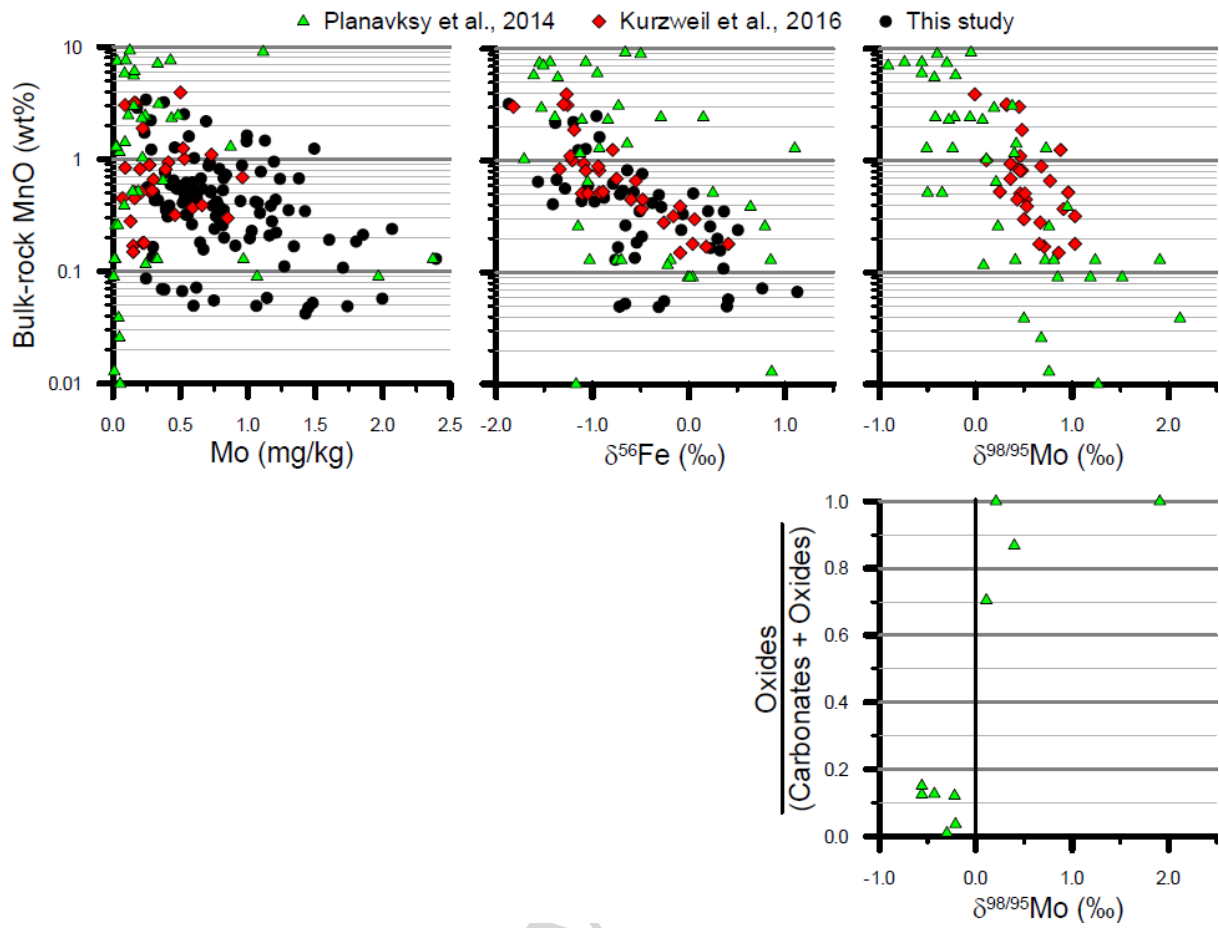


Fig. 9

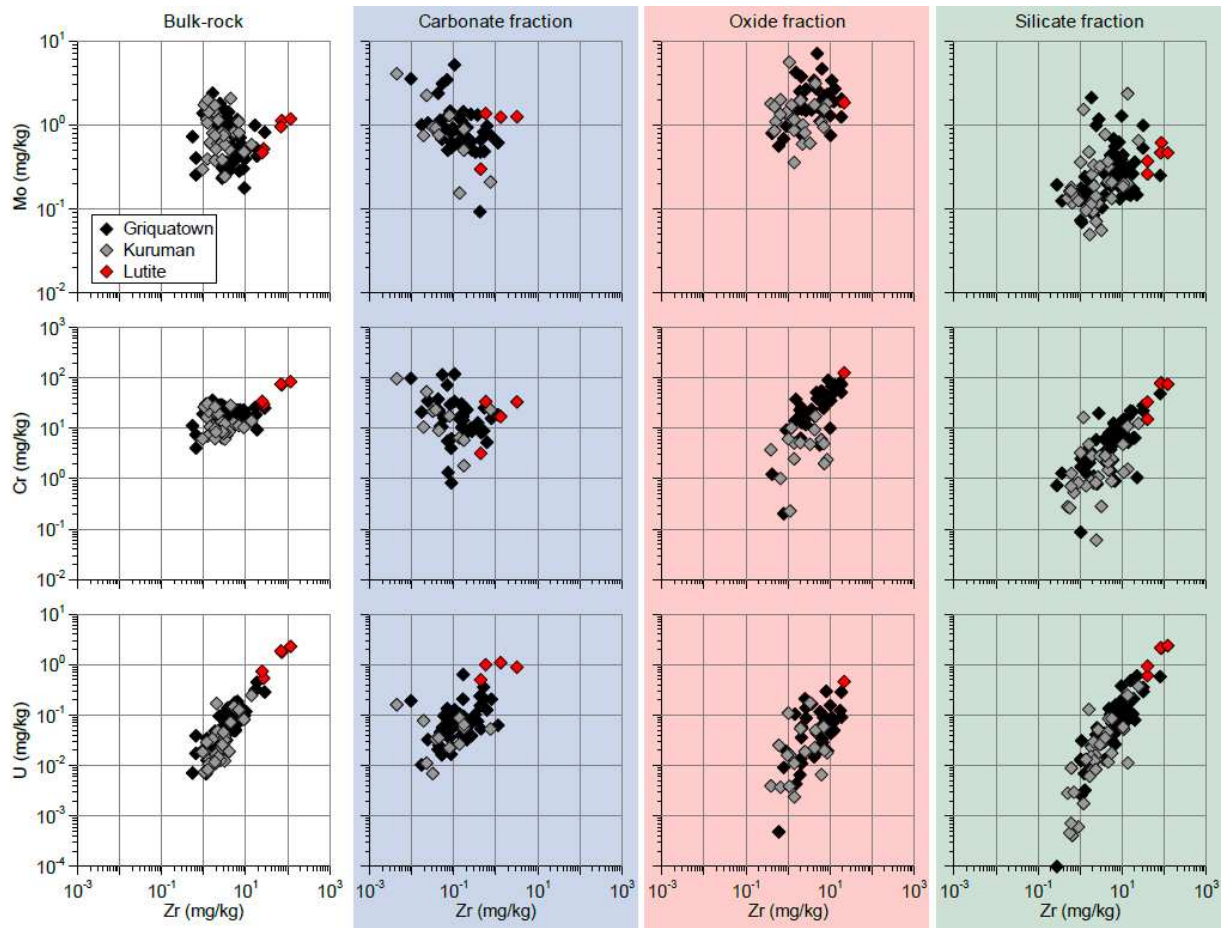


Fig. 10